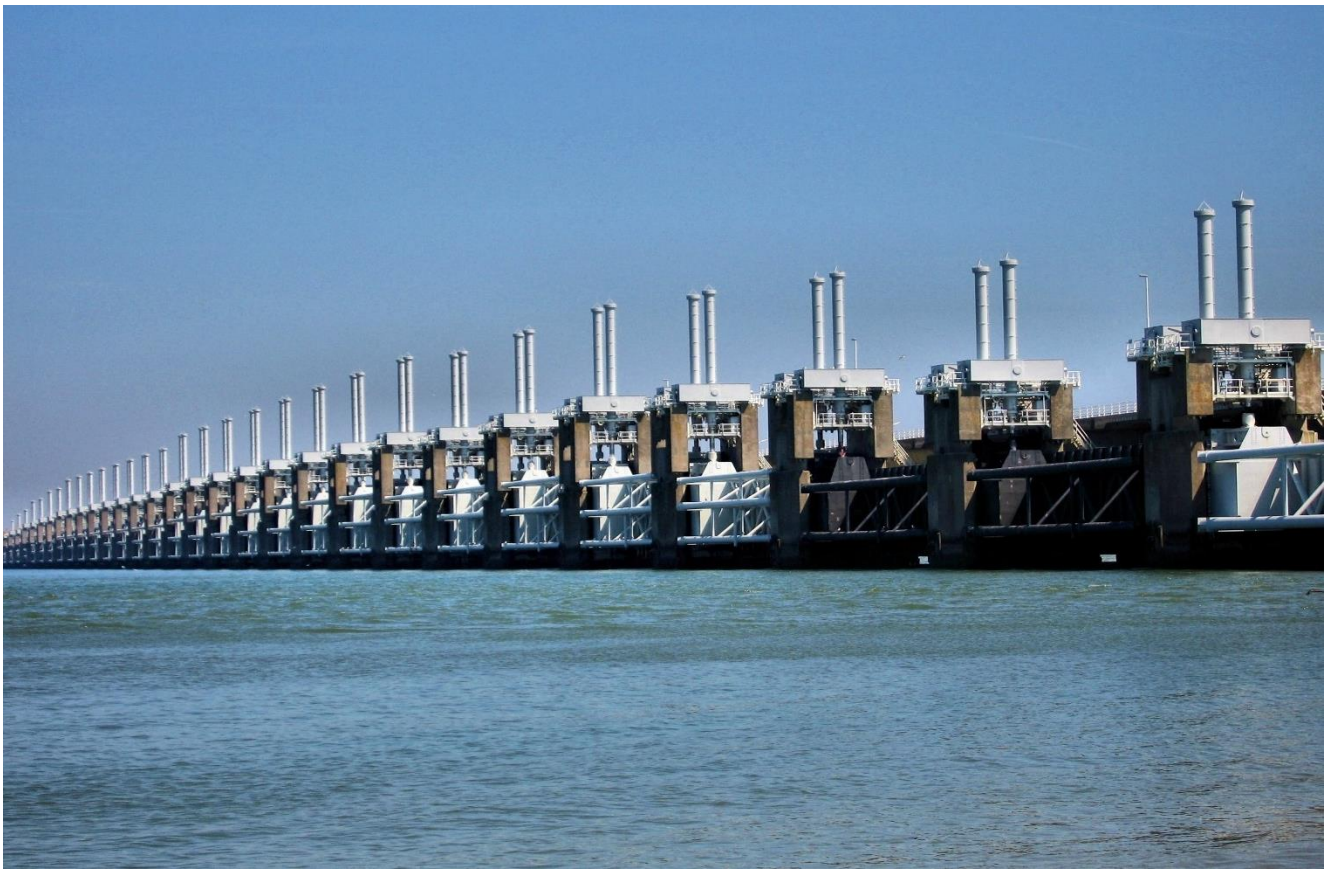

Pore pressure distribution in static liquefaction induced failure

Rutger Buitenhuis
Applied Earth Science

Pore pressure distribution in static liquefaction induced failure

Rutger Buitenhuis

BSc Thesis, Applied Earth Science
Student number: 4321294
Supervisors:
Dr. A. Askarinejad
Prof. Dr. M.A. Hicks
A. Maghsoudloo

Department of Geoscience & Engineering
Delft University of Technology
Februari 2019

Abstract

This bachelor thesis is dedicated to static liquefaction induced flow slides in the scour holes near the foundation of the Eastern Scheldt storm surge barrier. Since the construction of this Dutch water defence structure in the Netherlands, scouring of the loosely packed sand endangers the protection layers of the foundation on both sides of the structure. The scour holes are formed after failure of the submerged slopes.

This project rebuilt the slopes of the Eastern Scheldt in the geoscience laboratory. The submerged slopes of the Eastern Scheldt are reconstructed by dredging a slope in a large tank (Static Liquefaction Tank) filled with around 1 meter of sand. The tank is almost 5 meters in length and 2 meters in width and height.

The slope failure in the Eastern Scheldt is related to static liquefaction flow slides, which is a complex failure mechanism. The main objective of this experimental study is to gain an understanding of the pore pressure distribution during the undrained phase of static liquefaction. The undrained phase can be defined as the first stage of liquefaction in which water is not allowed to flow out during loading of the sand and all the load is carried by the pore water what reduces the soil's strength. For initiating static liquefaction induced flow slides there is a triggering mechanism necessary to bring the granular material in a region of instability. The instability can be reached after certain stress level in the sand is exceed. The triggering mechanism used in this experiment is water injection from the base of the Static Liquefaction Tank.

The simulation of the pore pressure distribution over time is by the use of a linear interpolation function. The interpolation function uses the data from the floating sensors in the sand to estimate the pore pressure development throughout the entire sand.
The results show that the upper most sensor closest to the surface of the slope are disturbed first by the base injection. Acceleration of the sand is initiated in the slope because the vertical effective stress drops suddenly to zero after a few seconds of triggering. The sudden decrease in effective stress causes the slope to liquefy and forms flow slides.

Contents

Glossary

Confining pressure: The minor principal stress acting on a soil specimen and in a triaxial test the confining pressure is applied by pressurizing the pore water in the specimen.
Deviator stress: Difference between the major and minor principals stress that act on a soil element in a triaxial test.
Drained phase: Conditions whereby the pore fluid is able to flow out of the soil and all the load is transferred on the soil skeleton.
Effective stress: Stress carried by solid particles of a soil and can be calculated by subtracting the pore pressure from the total stress.
Failure points: Locations instabilities inside a slope of granular material where initiation of static liquefaction induced flow slides may form at a microscopic scale.
Peak shear stress: Maximum value of shear stress before failure.
Plastic deformation: Deformation that is irreversible and will not return to its original state.
Pore water pressure: Stress carried by the pore fluid in the soil
Pressure chamber: A pressurized vessel that injects water to the base of the static liquefaction tank.
Shear strength: The ability of a material to resist external shear loading until failure.
Shear stress: The resistive force developed in a body due to an applied shear force.
Static liquefaction: Strength loss in a soil due to undrained failure.
Liquefaction tank: Experimental tank in the geoscience laboratory to perform test that simulates the static liquefaction induced flow slides.
Total stress: The total force per unit area within a mass of soil
Undrained phase: Conditions when pore water is unable to drain out of the soil. The load is all transferred to the pore fluid and the soil loses its strength.
Yield stress: Amount of stress a soil element needs to deform plastically or permanently.
Yield surface: Describes the boundary in stress state from elastic to nonelastic behavior.

1 Introduction

1.1 Problem description

The Deltaworks, one of the most impressive series of sea defence projects in the southwest of the Netherlands. One of the largest structures of the Delta Works is the Eastern Scheldt storm surge barrier. The Eastern Scheldt storm surge barrier consists of dams and storm surge barriers, which have been designed to protect the Netherlands from the future threats of high water from the North Sea.
Recent investigations have shown that strong scouring takes place at both sides of the Eastern Scheldt storm surge barrier. The turbulent flow of water through the storm surge barrier has the ability to raise erosional forces to the loosely packed sandy subsoil of the estuaries. Also, tidal changes in the Eastern Scheldt can lead to regions of potential instability due to deviating ground water movements in the subsoil. These scouring holes are located at the end of the 600m wide bed protection of the structure and endanger the future stability of the storm surge barrier. Over the years, these scour holes developed up to 34m depth in a period from 1985 to 2012 and are still ongoing. One of the major failure modes of the retrogression of the scour holes towards the barrier is static liquefaction induced flow slides. The non-cohesive loosely packed submarine sandy slopes in front of bed protection are susceptible for liquefaction-induced failure, in which the soil loses completely its strength and liquefy. The exact cause of the large excavation of sands near the bed protection of the Eastern Scheldt storm surge barrier is still relative unknown and challenging problem. For investigation of the large scour holes and flow slides, the TU Delft in cooperation with Rijkswaterstaat built a large-scale test facility (Static Liquefaction Tank) at the geoscience laboratory for research and test solutions for the problems close to the Eastern Scheldt storm surge barrier.

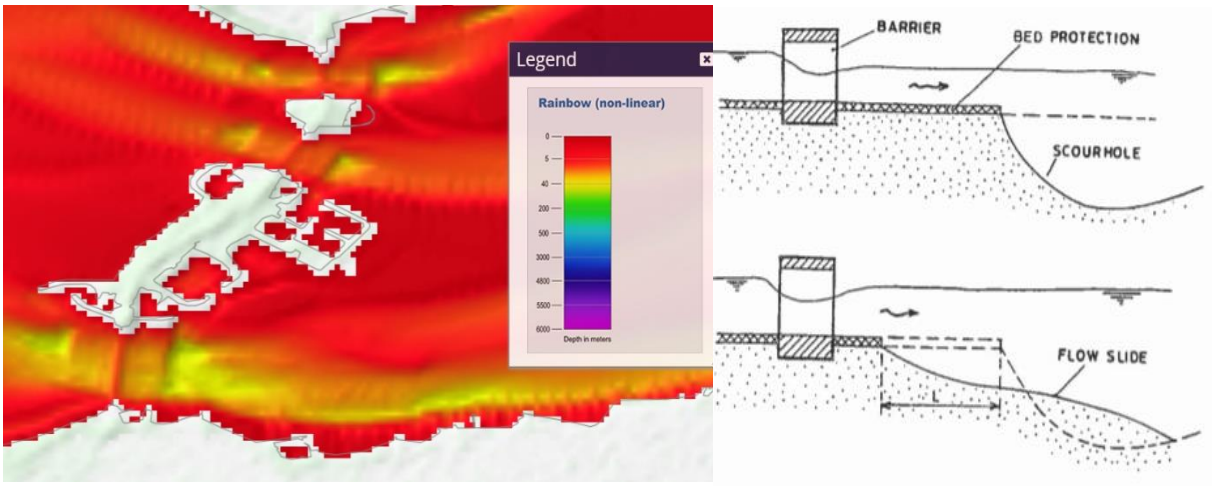

Figure 1: Bathymetric map (left) and process of scouring (right)

1.2 Research question

The main research question addressed in this bachelor thesis reads:

"What is the effect of base triggering on the pore pressure distribution throughout the sand during undrained conditions?"

The research approach involves answering the following sub questions:

1. Wat is static liquefaction and how is it related to strength loss in loosely packed sands in the Eastern Scheldt.
2. What is the effect of base triggering by water injection on excess pore pressure distribution throughout the sand under undrained conditions?
3. What is the effect of base triggering by water injection on the vertical effective stress in the sand?

2 Field description

Static liquefaction flow slides are a phenomenon occurring in loosely packed fine sands. These massive failures are a major threat for many submerged slopes nearby dikes and offshore structures. The subsoil of the Eastern Scheldt, a former estuary of the province of Zeeland, consist of alternating layers of more densely and loosely packed sands. Static liquefaction plays an important role in the failure of these loosely packed sands.

The geology of Zeeland is the results of erosion and sedimentation mechanisms during the geological history in the former estuaries of the Netherlands. A local profile of the subsoil in the Eastern Scheldt provides the following lithostratigraphic data near the barrier (Dinoloket, sd).

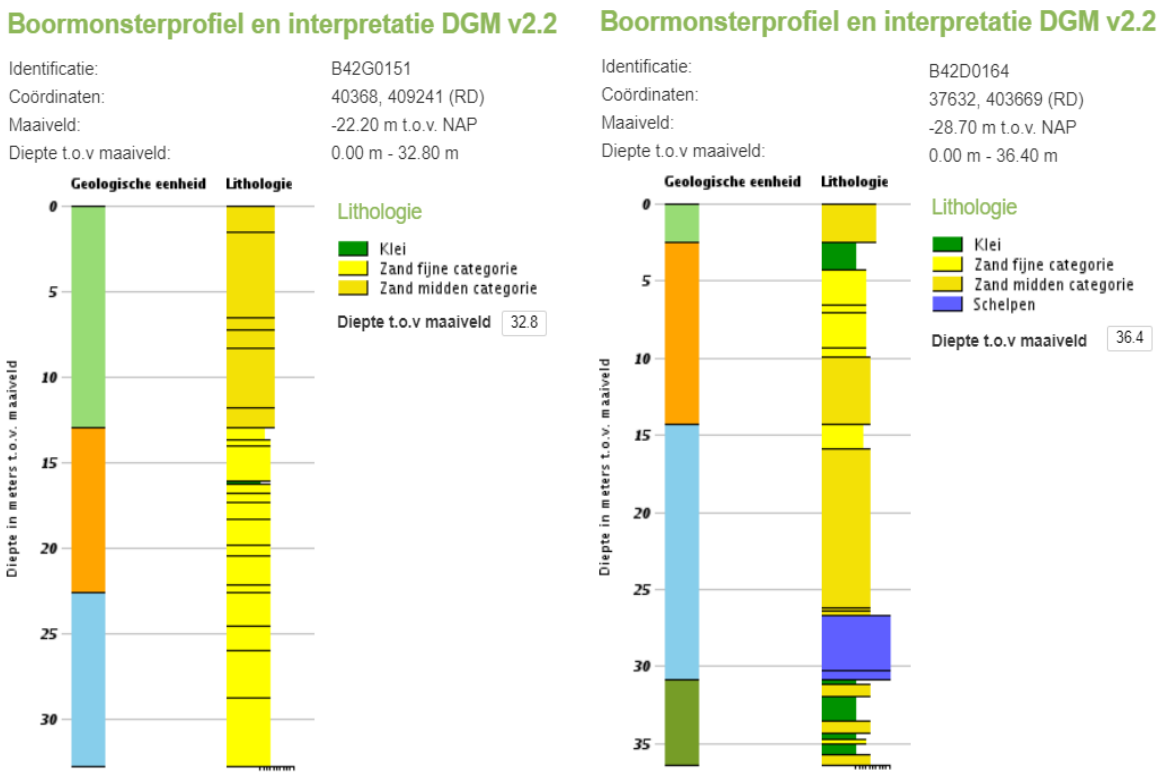

Figure 2: Borehole profile from location 1 (left) and 2 (right)

In the column under lithology ("Lithologie") the light-yellow part are fine sands. The green parts are clay and the dark-yellow parts are medium sands. These are the major types of material in every indicated section while silts could be present in between the sand particles.

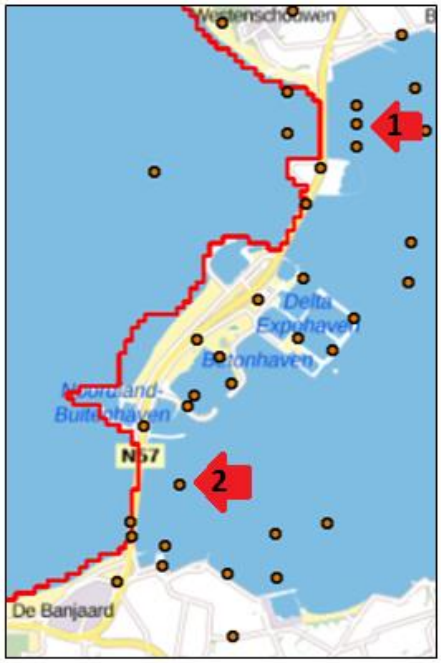

Figure 3: Locations of the borehole profiles from figure 2

Figure 3 indicates the location of the boreholes. The North Sea is located on the left side and the Eastern Scheldt at the right side of the figure. There are more bore hole profiles available on the map, but the chosen bore holes from Figure 2 are the deepest ones and close to the scour holes (Figure 1).

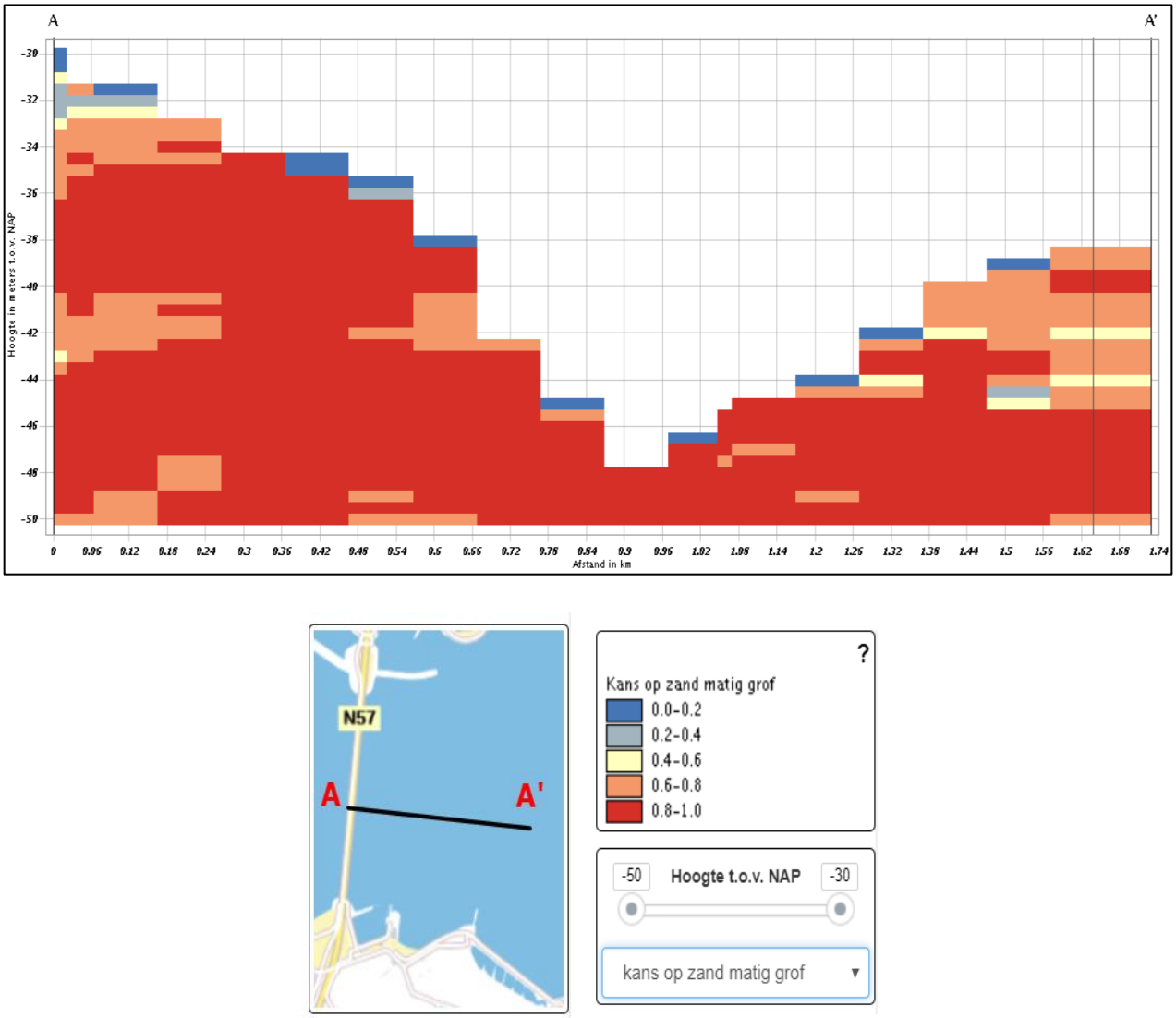

Figure 4: (Top) Colormap of probability of a certain particle size (red=80-100%) and (Bottom) the location of cross section

Before the construction of the Delta Works, the estuaries were subjected to both tidal forces of the sea and the rivers. The sedimentation of material in the tidal channels of the Eastern Scheldt occurred very quickly without strong wave action. As a result of the quick deposition of river sediments, the soil matrix is in a very loosely configuration and is therefore susceptible to liquefaction after small disturbances (Silvis & de Groot, 1995). Figure 4 shows the high probability of finding medium sized sands in the submarine slopes at location 2 (210-300µm). The dark blue points of the crossection are regions consisting relative more fine sands with silts. The exact date of the profiles is not yet known. Because of the dynamic behaviour of the subsoil due to breaching and liquefaction flow slides, the profiles are just an indication.

As described before, the sumbarine slopes consist alternating layers of densely packed sands and loosely packed sands. A schematic overview of the layering is prodived in figure below.

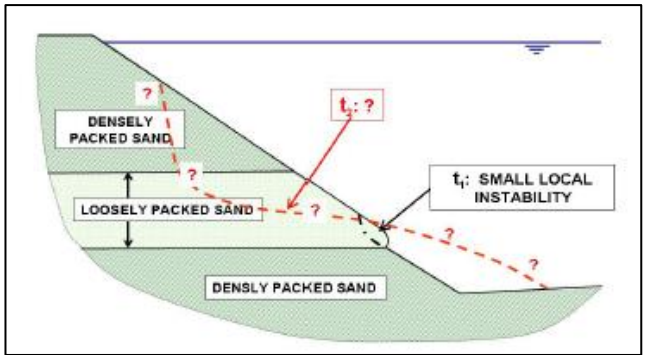

Figure 5: Overview of the configuration of the submerged slopes in the Eastern Scheldt (de Groot, Lindenberg, Mastbergen, & van den Ham, 2012)

Looking on a larger scale, Figure 6 shows the median diameter (D50) of the particle size distribution of the Eastern Scheldt. The figure also shows the particle distribution in the region of the scour holes in front of the barrier.

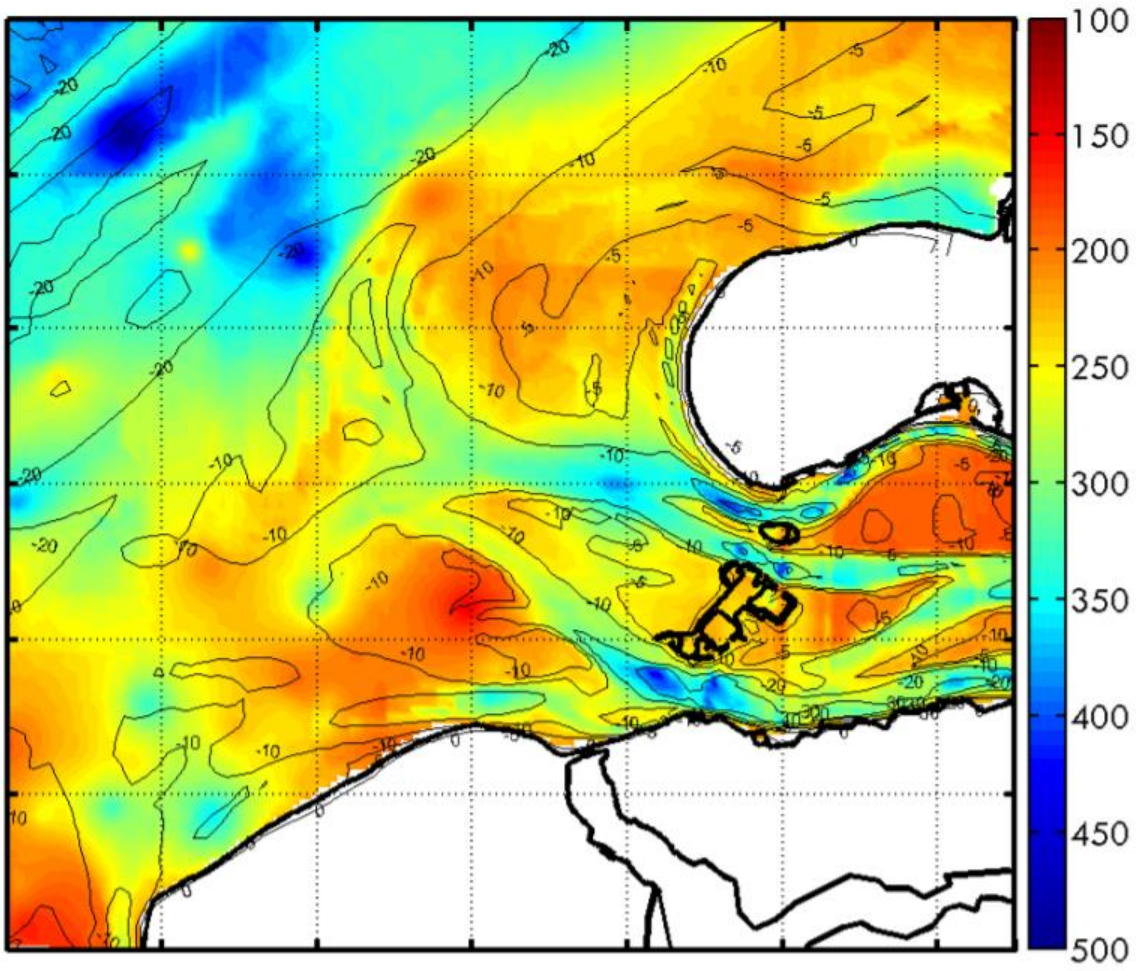

Figure 6: D50 at different locations in the Eastern Scheldt (D50 is in microns). Contour lines are based on bathymetry of 2008 (Eelkema, 2013)

Looking closer to figure, relative coarse material (D50 <> 400µm) is present at the bottom of the scour holes and more fine material can be found on the slopes or shoals (D50 < 250 µm) (Eelkema, 2013). The bottom of the Eastern Scheldt mainly consists of fine and medium sands ranging from 150 -200µm in size (Huisman & Luijendrijk, 2009). It has to be considered that due to heterogeneity in the subsoil because of post liquefaction conditions, this map gives a rough indication of the D50 present at different location.
The largest part of the subsoil in front of bed protection from the barrier is from fine to medium coarse sand. The figure below shows the susceptibility for liquefaction based on the particle size and percent of fines. For regions in the subsoils that are relative uniform, the grain size distribution curve falls in the region of high susceptibility for liquefaction. The reason behind this susceptible behavior is that in a poorly graded soil matrix, less effective grain-to-grain contacts forces are available, resulting in a lower strength of the soil.

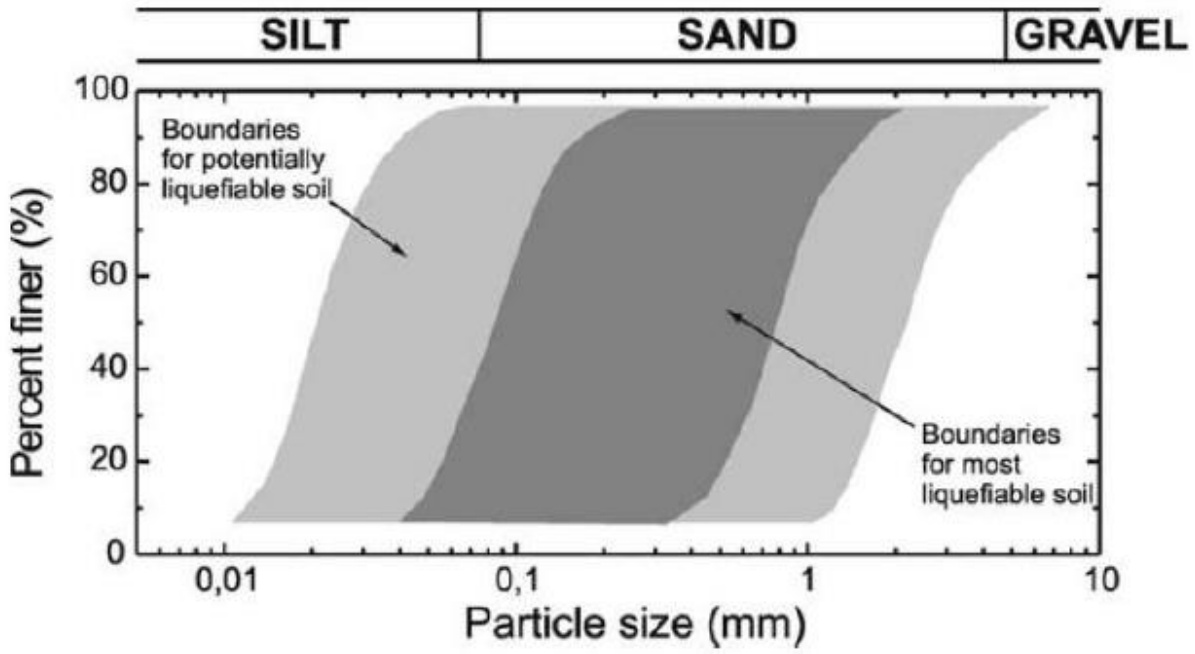

Figure 7: Ranges of grain size distribution for liquefiable soils (Tsuchida, 1970)

2 Static liquefaction in submerged slopes

In the Dutch Water Act it is described that the primary flood defences along the estuaries, coasts and rivers have to be evaluate and assessed for their reliability every 6 years (van der Krogt, van den Ham, & Kok, 2015). Several failure mechanisms could endanger the future stability of the flood defences. For example, dikes may fail by different mechanisms such as backward internal erosion, overtopping, slip failure or damaged revetment (protection layer) and are positive correlated to the water level. Another failure mechanism, also called failure modes, is flow sliding and may also lead to flooding in the foreland near the structures of the flood defence. In the Eastern Scheldt, flow slides forms one of the major failure modes of slope failure of the submerged slopes of very loose sands and silts. Regarding flow slides, two types of failure mechanisms are important: static liquefaction and breaching in which both forms a turbidity current and resediments under a very gentle slope. The occurrence of flow slides is not related to water levels and will therefore not directly lead to flooding. On the other hand, flow slides affect the failure probability of the direct failure modes and decrease the reliability of the protection bed of the Eastern Scheldt in the future (van der Krogt et al., 2015). To explain the concept of static liquefaction flow slides in more detail, this chapter is devoted to the simplified fundamentals of static liquefaction flow slides.

2.1 Definition of static liquefaction

Liquefaction is one of the major problems in geotechnical engineering. A formal definition of liquefaction can be stated as a phenomenon in which a loose saturated or partially saturated soil loses strength and stiffness in response to a sudden change in the stress conditions on that soil after a triggering event. In granular material, such as sands and silts, the sudden strength loss is due to the undrained conditions, in which all the loading is temporarily transferred to the pore water and the effective stress reduces to zero. The generated excessive pore water pressure liquefies the granular material and causes flow slides. Once the particles are liquefied, the strength of the soil is restored when the sediments settle down through the pore fluid and grain-to-grain contacts are re-established (Owen & Moretti, 2011).

Triggering mechanisms that could initiate liquefaction in the laboratory are for example vibrations and additional pore pressure injections. In nature, the triggering may be caused due to man-made activities (constructions), earthquakes, local erosion, tidal variations or overloading by additional fill. All these (minor) disturbance could be considered as the origin to the sudden increase of the pore water pressure in the soil (Lade & Yamamuro, Static instability and liquefaction of loose fine sandy slopes, 1992). Later on, the triggering will be discussed in more detail.

2.2 Basic soil properties

Before describing the process of liquefaction, a short introduction to some basic soil properties could be convenient. In general, the characteristic of a soil is that is consist of multiple phases such as solids, liquid and gas and in which its properties depend on the interaction between these phases and the applied stress on it. Soil is comprised of three major components in which the solid particles forms the soil skeleton and the voids are filled with water and/or air. In the Eastern Scheldt, the soil is saturated what means that the voids are entirely filled with water.

In geotechnical engineering various soil parameters can be used to describe the soil texture.
In the field of liquefaction, the most important parameters are the void ratio, relative density and grains size distribution. The grain size distribution of granular soils defines the relative amount, typically in mass, of the particles present in a soil sample. As described before, relative uniform and fine soils are more susceptible for liquefaction than coarse and poorly sorted soils, because in a more non-uniform soil there are more contact forces between the particles and in a coarser soil the liquefaction resistance increases because of improved drainage. Therefore, clarifying the gradation curve of liquefiable soils is an important approach to describe the static and dynamic behavior of the soil. Other soil properties such as the void ratio and relative density also influence the liquefaction potential. For example, in a triaxial *cyclic* loading test on uniform Toyoura sand, shows that in general the resistance to liquefaction increases with an increase in relative density. The liquefaction resistance increases linearly with relative density up to 70% and above 70% the strength went up sharply (Hoque, Ansary, & Yasin, 2017). These Toyoura sand (Dong, et al., 2015) can be compared to a certain extent to the fine sands in the liquefaction tank because of similarities in grain size distribution (D50), uniformity coefficient and maximum and minimum void ratio.

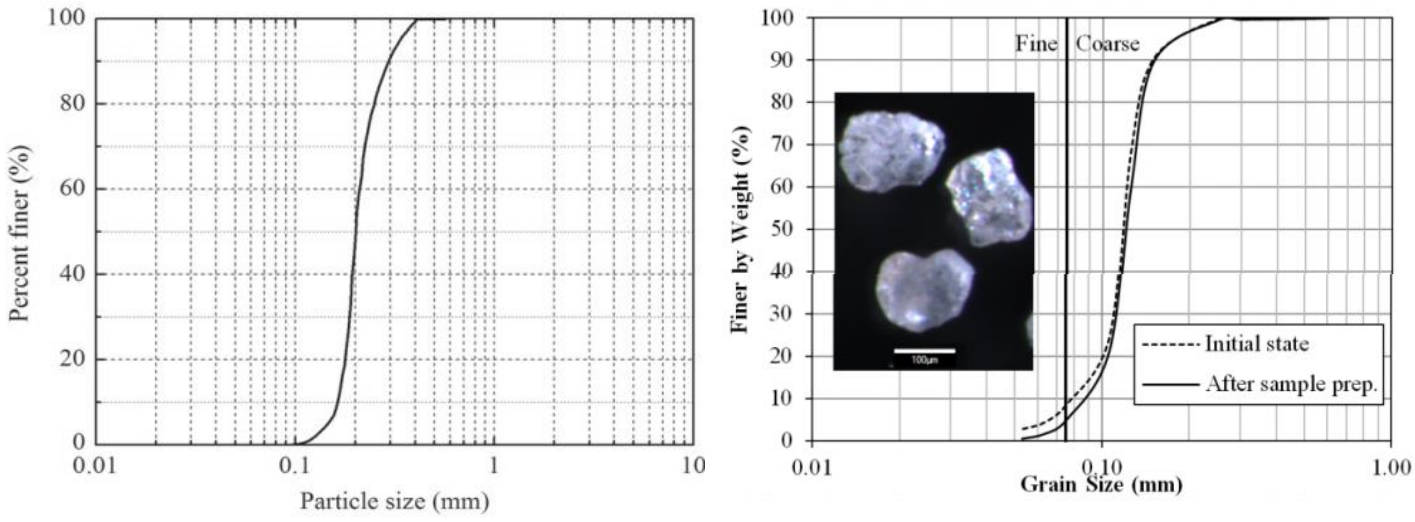

Figure 8: Grain size distribution Toyoura sand (left) and Geba sand used in SL tank (right) (Maghsoudloo, Askarinejad, de Jager, Molenkamp, & Hicks, 2018)

The relative density can be calculated by using the following formula:

[1] $$D_r = \frac{e_{max} - e}{e_{max} - e_{min}}$$

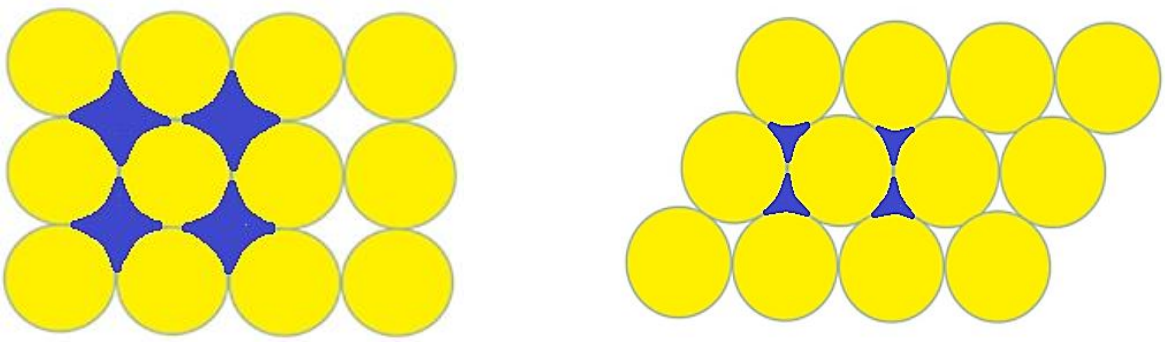

Figure 9: Loosest Possible configuration (e min, RD = 0%) left and densest possible configuration (e max, RD=100%) right

By laboratory tests the minimum and maximum void ratio can be determined. In the experiments, the void ratio of the tested sand body in the liquefaction tank is derived by:

[2] $$e = \frac{G_s \rho_w}{\frac{m_{sand}}{V_{sand} * 1000}} - 1$$

In which G_s is the specific gravity (2,67), ρ_w the water density (1,00 g/cm3), m_{sand} updated sand mass (kg) and V_{sand} the volume of sand (m^3). The volume is calculated by:

[3] $$V_{sand} = A_{tank} * h_{sand} + V_{grid}$$

The area of the tank is 9,424 m^2 and the volume of the grid 0,225 m^3. By changing the height of the sand body (h_{sand}) the desired relative density can be obtained.

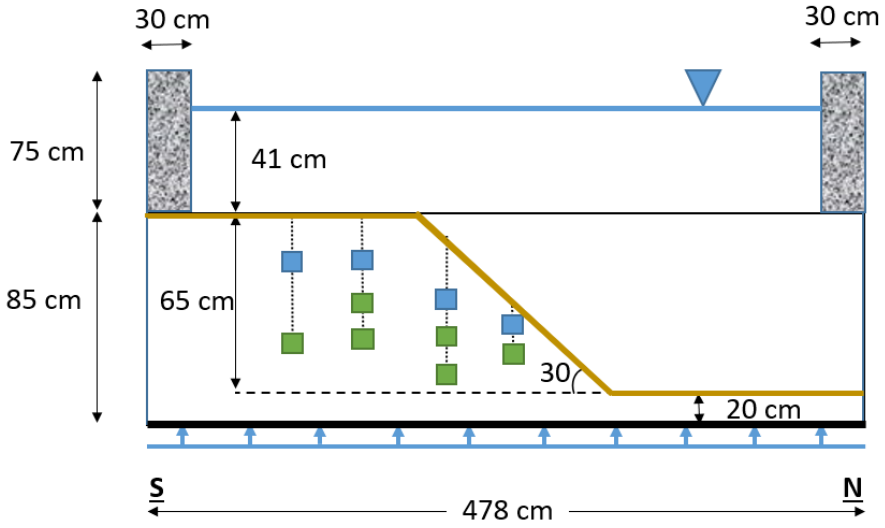

Figure 10: Side view of the SL tank

3 Soil instability

Before static liquefaction can be explained in more detail. A good understanding about the state of stresses in a slope is necessary. Furthermore, the mechanics of instability inside a soil is described and finally this chapter explains the determination of regions of potential instability that could lead to liquefaction. Localizing the regions of potential instability after triggering is also part of the experiments done in the liquefaction tank.

3.1 Mechanics of instability inside failure surface

The mechanics of instability in granular soils is a requirement for describing the phenomena of liquefaction in submerged slopes. In a more geotechnical sense, instability can be stated as the inability of a granular material to sustain or carry a given load and next to that the inability of the granular material to sustain small perturbations in the load on the soil matrix (Lade & Yamamuro, 2009).

Earlier studies (Lade & Yamamuro, Static instability and liquefaction of loose fine sandy slopes, 1992) have shown that whether the volumetric change in a granular material, such as in sand, is contractive (tendency to compress) or dilative (tendency to expand), the soil will be stable before failure points are created if drained conditions are applied. In experiments in which the stresses were controlled, during shearing a contractive and fully saturated sand could become unstable inside the sand if undrained conditions are prevailed. In the beginning of those experiments, loading on the specimens was done under drained conditions to pre-defined stress levels (S). The stress level can be explained as the ratio of the current difference to maximum stress difference at a given confining pressure. At failure points, the ratio is 1. In the same experiment, after the drainage valve was closed, instability developed in the specimens because of an increment in pore water pressure during loading. Therefore, the stress level increased because of an increase of pore water pressure in the specimen and a decrease of the effective confining pressure. Other experiments (Peters, 1991) showed that a partly saturated fine sands or silts with low hydraulic conductivity can become unstable if the degree of saturation is high enough and the loading conditions are changed fast from drained to undrained. In comparison to contractive sands, also dilating sands and silts may become unstable if the (negative) rate of volumetric expansion of a small sand element exceeds the negative rate of expansion exhibited by the sand. In this case, the effective confining pressure also decreases and the sand element is not able to sustain the applied shear stress. Concluding, a negative or positive rate of volume change to a soil element can lead to instability depending on the rate of volume change exhibited by the entire soil, what could be a dilative or contractive behaviour.

3.2 Region of potential instability

In the previous part it is mentioned that loading of a contractive soil can lead to unstable behaviour during undrained conditions. The subsoil of the Eastern Scheldt consists of silts and sands (see borehole profiles in Chapter 1) with a loose packing and a relatively low hydraulic conductivity. Small disturbances in loading can activate undrained conditions resulting in instability in the soil. When the soil has reached a condition for instability, the soil may not be able to sustain the present stress state. The instability at a certain stress state is associated to the top of the current yield surface. In Figure 11 this is schematically shown in a p'-q diagram.

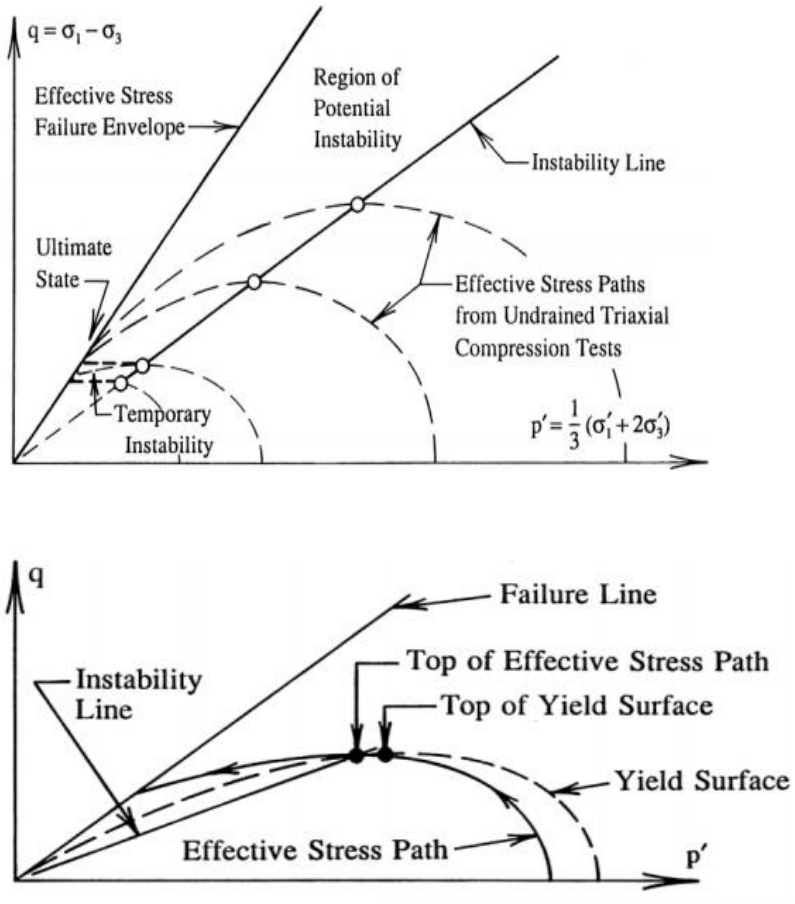

Figure 11: Location of instability line for loose sand (Lade & Yamamuro, 2009)

In the p'-q diagram, the p' stands for the effective mean normal stress and the q is the deviators stress (σ1 – σ2). The top of the undrained effective stress paths (empty dots with $(\sigma 1 - \sigma 3)_{max}$), occurs slight after the yield surface top. The line between the yield surface tops provide the lower limit of potential instability. From that point, the soil can deform plastically under decreasing stresses. Instability in a granular material occurs if the state of stress is located on or above the instability line. The instability line intersects the origin of the stress diagram. Shown in upper graph of Figure 11 There is also a region of temporary instability where instability may occur, but conditions allow the soil to become stable again. This is located in the upper zone of the dilating zone, but when the soil is able to cross the transformation line (from contraction to dilation tendency) the material becomes stable again Figure 15. In very loose sands, that may concern the Eastern Scheldt subsoil, the region of potential instability reaches the origin of the diagram (Lade & Yamamuro, 2009). The failure of the soil could occur at the effective stress failure envelope line that intersects the q-axis. Liquefaction does not occur if temporary instability is reached, because the frictional strength will recover with further straining (Sladen, D'Hollander, Krahn, & Mitchell, 1985).

3.3 Instability and liquefaction

Instability and liquefaction occur in cyclic and static loading. Initiation of instability in a soil, in specific a soil element, requires that the stress state at some points are in or brought into the region of potential instability. As long as the process is drained, the soil will remain stable at failure points. A cause of instability may be a triggering mechanism that increases in pore pressure for a short moment in which the excess pore pressure has no time to dissipate. For loosely packed sands, the instability line itself is not a principal triggering mechanism for instability, because sands are stable above the instability line if drained conditions prevail. Under static or cyclic loading, the initiation of instability occurs at very low amount of strain. At a certain moment when the instability has been triggered, it could lead to liquefaction at large strain, as shown in Figure 13. Because the triggering initiates the instability at small strains in the sand, the initial grain structure has its effects on the susceptibility for liquefaction. Summarizing, the initiation of the instability occurs at small strain and can result in liquefaction what involves larger strains. This describes the correlation between the grain structure, which can only affect the behavior of the sand at small strains and liquefaction what occurs at large strains in which the effects of the initial grain structure would be negligible (Lade & Yamamuro, 2011).

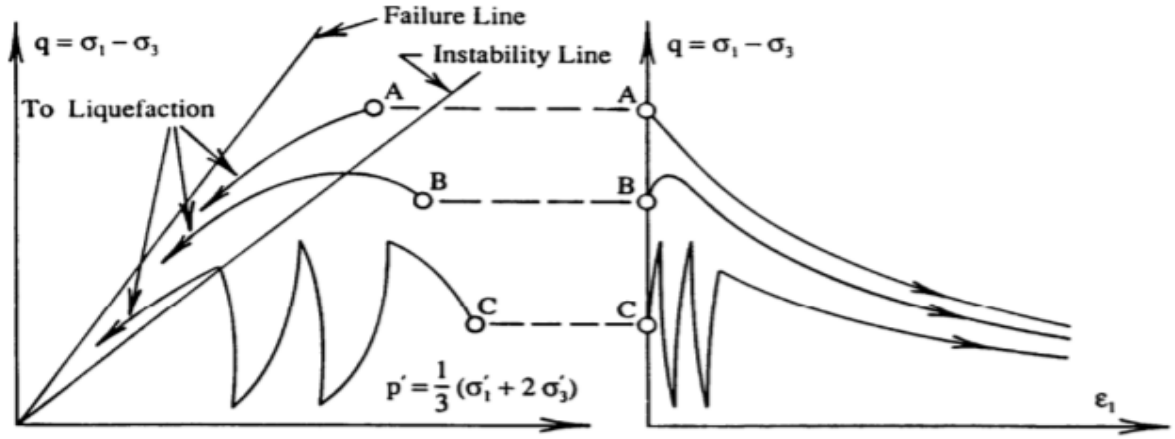

Figure 13:Diagram showing stress paths (a) and stress-strain relation (b) for initiation of static (A,B) and cyclic (C) instability at small strains and the resulting liquefaction at large strains under undrained conditions in loose sands. ϵ1 is major principal stress

3.4 Mechanics of static liquefaction

In chapter 2 field description, it was assumed from borehole loggings and cross-sectional data that the subsoil of the Eastern Scheldt mainly consists of fine sands with silty particles in between. For explaining the process of liquefaction, the mechanics beyond it are based on the structure and properties of liquefiable silty sand deposits, what are in the range of the expected depositions that can be found one the submerged slopes in the Eastern Scheldt.

3.4.1 Structure and properties of liquefiable silty sand deposits.

The structure of a loosely packed fine silty sand is showed in Figure 14. On the sample at the right-side of the figure stresses are applied and causes the smaller silt particles to move into the void space, resulting in a significant volumetric contraction and that may cause liquefaction. The stiffness of the soil matrix increases as the large grain particles are brought into contact.

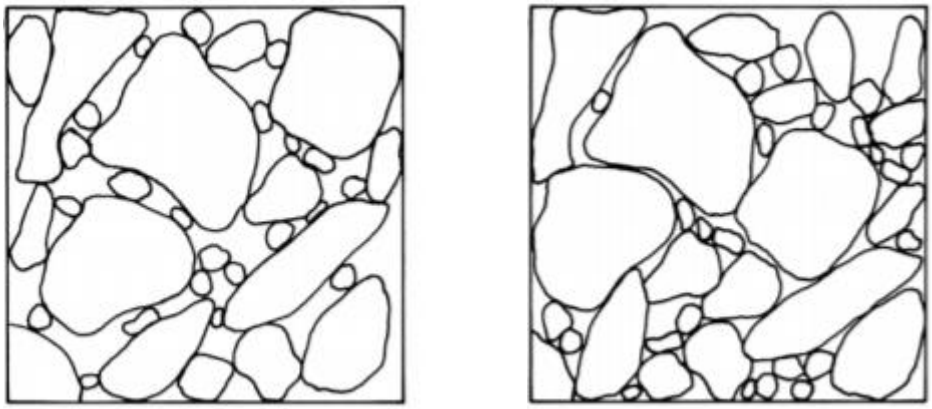

Figure 14: Diagram showing silty sand deposit in loose state (left) with larger/smaller sand/silt particles. Right is a more compressed and sheared configuration (Lade & Yamamuro, 2009)

Local collapses in the structure of the loose soil induce a contractive tendency and causes the pore water pressure to increase, in which the effective stress is reduced, and further structural collapse is induced. On the other hand, the collapses allow the larger particles to create more contact points between each other and therefore increases the frictional resistance to deformation. In a loosely packed silty sand, the structure allows the sand particles to contract easily at low confining pressures. This property allows that the increase in pore pressure becomes sufficient large in such a way that the effective confining pressure reduces to zero and liquefaction could occur. When the effective pressure reduces close to zero, the structure between the large particles is has not been completely lost and recovers its frictional resistance and strength as straining continues. In Figure 15 this is shown by a triaxial test on a Nevada Sand with a relative density of 12% (reaching loosest possible configuration). The figure also shows that a sample with an initially larger effective confining pressure has a higher capacity to absorb rising pore pressures and resulting in a stronger resistance against static liquefaction (Lade & Yamamuro, 2009).

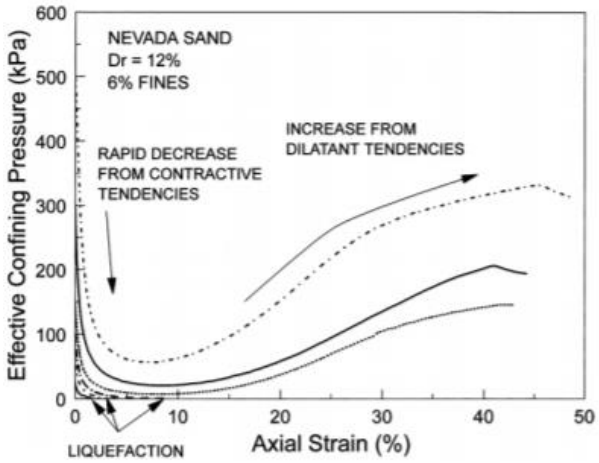

Figure 15: Relation between initial effective confining pressure during a shearing test (Lade & Yamamuro, 2009)

In the undrained triaxial test in Figure 15, low ranges of initial confining pressures show that the effective confining pressure reaches faster zero with declining initial consolidation pressure. Concluding that the lower the initial consolidation pressure, the faster conditions for liquefaction are reached in a soil. Besides that, it confirms that static liquefaction is a low-pressure phenomenon. An increase in confining pressure has its effect on an increase in resistance for liquefaction.

The behavior of very loose silty sands at low confining pressure can be seen in Figure 16.
In comparison to conventional undrained tests, a 'reverse' behavior can be seen in the figure in which at low confining pressure in a silty sand specimen is accompanied by an inflection in the instability line. Different types of effective stress paths with their patterns are shown in the figure. At the lowest pressures, static liquefaction occurs and is characterized by development of large pore pressures what reduces the effective confining pressure to zero and zero stress difference at low axial strains (Lade & Yamamuro, 1997).
The inflection can be explained as a region in which shearing continues, and the stress path crosses the phase transformation line resulting in a zone of dilation with a declination in the pore pressure. The increase in stress difference is at much higher magnitudes than initial peak.

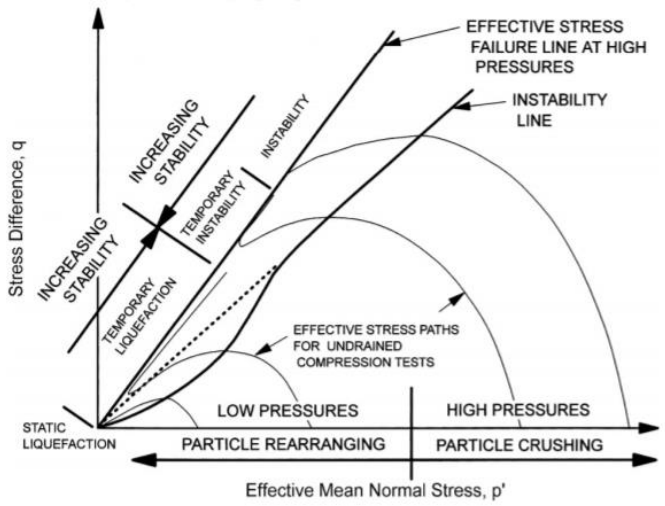

Figure 16: Different types of undrained effective stress paths for loosely packed silty sands: static liquefaction, temporary liquefaction, temporary instability and instability in a p'-q diagram (Lade & Yamamuro, 2009)

Furthermore, under undrained conditions the development of pore pressure is directly related to the compressibility of a soil. Tests on loosely packed silty sands demonstrate a significant volumetric contraction at low pressures. The 'reverse pattern' of the sand behavior is completely controlled by the large amount of fines resulting in high compressibility in loose silty sands.

3.4.2 Analysis for static liquefaction in a submerged slope

For analyzing the potential of a slope for static liquefaction, the current state of stress at every point in the slope has to be compared with the state of stresses in the region of potential liquefaction shown in the p'- q diagrams. By using the instability method for a submerged slope, the state of stress in a slope are overlapped on the stress diagram to determine if any stress state falls into a region of potential instability. In the case over overlapping, every point in the slope becomes a location of potential instability and under undrained conditions the instability will develop. At the same time a convenient triggering mechanism may activate the initiation the instability.
The slope may liquefy if the stress state is in a region of potential instability and the critical region is all the way down to the stress origin in the diagram, where true static liquefaction take place (Lade & Yamamuro, 1992).

3.4.3 Zone of potential liquefaction in submerged slope

Identifying the states of stress in a submerged slope with moderate inclination (approximately angle of repose) can outline a zone in which liquefaction might be triggered. The horizontal effective stress can be obtained by using the coefficient of earth pressure at rest, K_0:

[4] $$\sigma'_h = K_0 \sigma'_v$$

[5] $$K_0 = 1 - sin\varphi$$

In which σ'_v is the effective vertical stress. The correspond Mohr's circle is shown in Figure 17

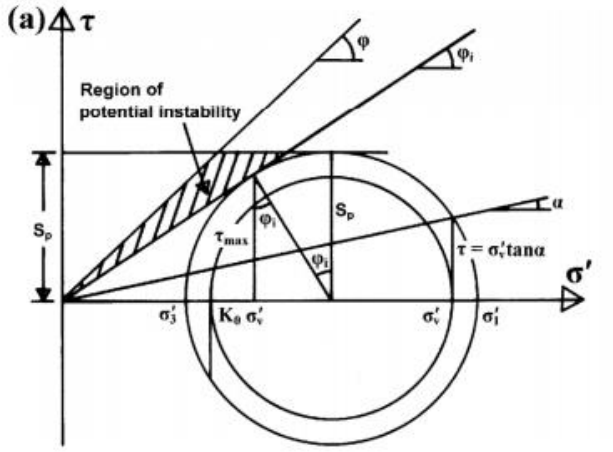

Figure 17: Mohr circle with indication of normal stress and shear stress limiting the region of potential instability (Lade & Yamamuro, 2009)

The Mohr's circle gives a good indication for the real stress states in a gently inclined slope. Although the Mohr circle for K_0 may not fall in the region of potential instability, by adding the shear stress due to inclination, the state of stress can be brought, at some points, into the region of instability.

The required slope inclination for the Mohr circle to become tangent to the instability line is formulated by the following expression:

[6] $$tan\alpha = \frac{1}{2}\sqrt{(2-\sin\varphi)^2 \cdot sin^2\varphi_i - \sin^2\varphi}$$

In which φ is the effective stress failure line and φ_i is the angle of the instability line.
Hence, for slopes with an inclination smaller than α, the Mohr circle will not achieve a region of potential instability and under static conditions it will not become unstable. Inclination larger than α, many points, or soil elements, in the slope will fall in the region of potential instability. In Figure 17 the region of instability is in that case limited to the peak shear stress S_p present in the slope.
The analysis to determine this region can be achieved by calculating the following physical quantities:

[7] $$W = hcos(\alpha)b\gamma_b$$

[8] $$\sigma = \frac{Wcos(\alpha)}{b} = \gamma_b hcos^2(\alpha)$$

[9] $$\tau = \frac{Wsin(\alpha)}{b} = \gamma_b hcos(\alpha)\sin(\alpha)$$

Where *W* is the weight of the soil volume that is being analysed, h the vertical depth below the sloping surface, b the length along the sloping surface, γ_b the buoyant unit weight and σ the effective normal stress on the base of the soil volume.

The peak shear stress can be expressed in terms of τ

[10] $$S_p = \frac{\sigma 1 - \sigma 3}{2} = \frac{\tau}{\cos(\varphi_i)} = \frac{\gamma_b hcos(\alpha)\sin(\alpha)}{\cos(\varphi_i)}$$

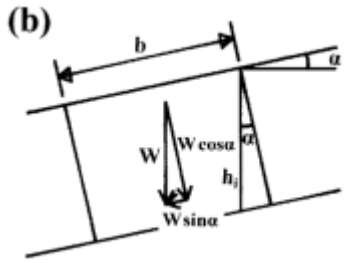

Figure 18: Volume of soil for calculating stresses along plane parallel to sloping surface (Lade & Yamamuro, 2009)

The vertical depth (h_i), from the sloping surface down to the zones of potential instability can be obtained from expression [10].

[11] $$h_i \leq \frac{S_p\cos(\varphi_i)}{\gamma_b\cos(\alpha)\sin(\alpha)}$$

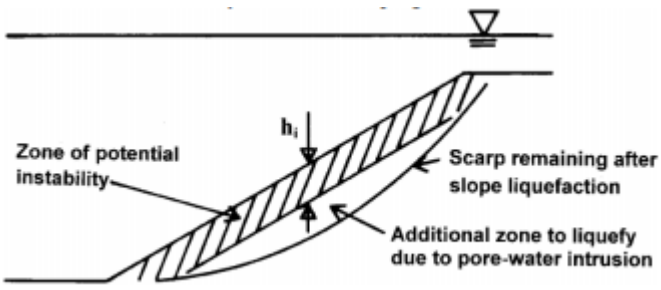

Figure 19: Indication for the zone of potential instability with h the vertical depth of the zone of instability below sloping surface (Lade & Yamamuro, 2009)

Concluding that the zone in which instability could be initiated reaches from the sloping surface to a vertically depth to h_i. Nevertheless, it has to be mentioned that the maximum inclination is limited to $\alpha=\varphi$. As long as the conditions are drained in $\alpha=\varphi$, the soil will remain stable. But small disturbances can cause, for relative low permeability silty sand, to become in undrained conditions and the slope will become unstable.

3.5 Triggering mechanisms

Failure of a sloping ground because of static liquefaction occurs once the shear stress applied by a monotonic triggering load exceed the undrained yield (peak) shear strength in the liquefiable saturated cohesionless soil. For initiating the static liquefaction flow failure and undrained stain softening a triggering mechanism is required. There are multiple triggering mechanisms that may initiate a sloping ground to failure and act on different location inside a slope. Figure 20 gives an indication of zones in which certain triggering mechanism can activate the slope failure.

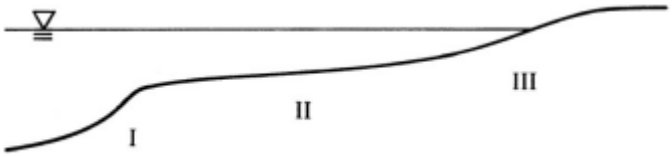

Figure 20: Zones inside a slope where instability might be initiated

Some types of triggering mechanism could activate failure in particular regions inside the slope. But most of the mechanisms are suitable triggers throughout the entire slope. For example, over-steepening at the toe due to scouring, rapid sedimentation or construction activities may initiate liquefaction in region 1. Overloading by construction activities or rapid sedimentation can affect all the regions 1,2 and 3. The same is valid for pore pressure changes due to soil compression, storm wave action and gas generation. Earthquakes and slope steepening due to tectonic tilting can also trigger all the regions. Seepage forces out of the slope due to low tides may affect more region 2 and 3. Slope exposure above ocean surface because of drawdown conditions may affect region 3 (Lade & Yamamuro, 2009).

4 Experimental study

4.1 The Static Liquefaction Tank

The experiment is performed inside the liquefaction tank at the Geoscience Lab.
The main purpose of the liquefaction tank is to simulate the process of static liquefaction flow slides that occurs in the Eastern Scheldt in the Netherlands.
The main focus of this project was to gain insight into the distribution of the pore pressure directly after base triggering in the sandy slope in the undrained phase of the process. Between the moment of initiation by triggering towards the acceleration of the sand particles, there is a short delay in time in which the soil is generating excess pore pressure. The excess pore pressure is able to bring the sand into a region of instability when a certain stress state is exceeded. The instability may bring the slope to failure and static liquefaction induced flow slides will be observed in the static liquefaction (SL) tank.

4.2 Objective

The main objective of the experiment is to simulate the distribution of the pore pressure in the sand slope after a triggering mechanism is initiated. The triggering mechanism used in the experiment is water injection from the base of the liquefaction tank. The simulation ends at the moment that the sand starts to show deformation. It is assumed that the undrained conditions end at the moment when the sensors in the sand starts to measure changes in acceleration.

4.3 Methodology

The methodology is divided into two sections. The first part describes the practical setup of the experiment in the laboratory and the second part explains the processing of the sensors data for making the simulations in MATLAB.

4.3.1 Practical set up

4.3.1.1 Sample preparation

The experiment starts with the preparation of the sand with a suitable relative density. The relative density can be calculated from equation 1 by measuring the height of the sand in the tank. For obtaining a uniform relative density through the sand, the sand is fluidized for a few rounds. From experience the best procedure was to fluidize the sand in two rounds in which the maximum sand height reached a height of about 125-130 cm during fluidization. After two rounds of fluidization, the desired relative density was in the range of 30–36 percent. The last step was to apply a shock of 3 seconds by the fluidization system on the sand whereby the relative density increases to a range of 40-48 percent. There are two points to be considered when obtaining a usable relative density. First, the sand must not be too dense or loose (40<RD<48), otherwise the sand will be high susceptible for (undesirable) liquefaction during dredging or too much densified that there will be no failure after triggering, respectively. The last point to note is that the relative density has to be reproducible, because in future experiments the sand has to have the same properties as previous experiments to draw better conclusions.

4.3.1.2 Dredging the slope

Dredging the sand mass is necessary for creating a sandy slope in the liquefaction tank. The suction at the dredging heads is based on the venturi effect. The venturi effect means a reduction in the fluid pressure in a pipe due to a constriction. When another smaller pipe is connected to the point of the constriction, there will be a negative pressure inside the smaller pipe and there will be suction generated at the other end of the smaller pipe.

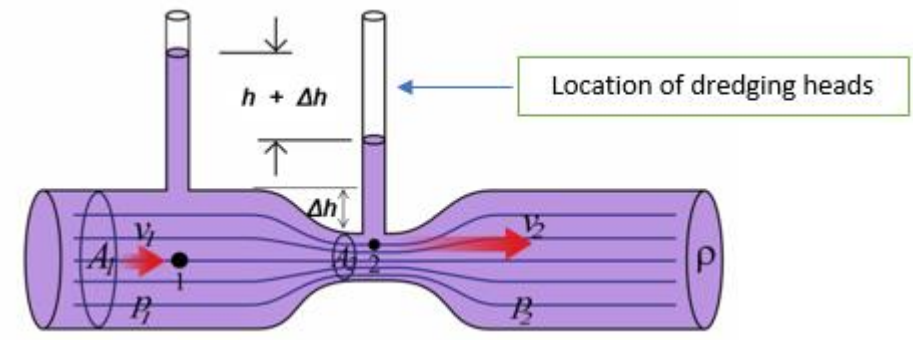

Figure 21: The venturi effect, based on Bernoulli's Law

The pressure difference between the constriction and larger section of the pipe can be described with Bernoulli's law in the following form:

[12] $$P_1 - P_2 = \frac{\rho}{2}(v_2^2 - v_1^2)$$

In which $P_1 - P_2$ is the pressure drop at the constriction, ρ the density of the fluid and v_1 and v_2 the velocity of the water in the larger tube and the constriction, respectively.

Dredging the slope is a time-consuming process and the dredging process itself is also a kind of triggering mechanism.

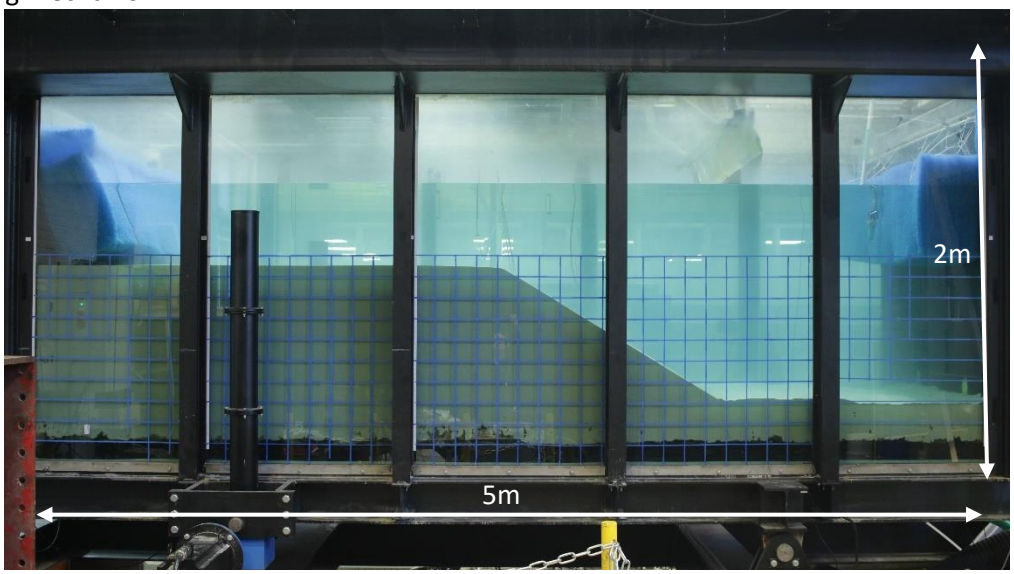

Figure 22: Shape of the sand before triggering

4.3.1.3 Base triggering

One of the most important steps in the entire experiment is the triggering mechanism that is used to bring the slope to failure. As described before in section 2.5 there are several mechanisms that can be used to trigger the slope. By testing, triggering by increasing the pore pressure by water injection was the most effective way. Also, vibration by a rod inside the slope was tested, but it had no influence on changing the stress state of the sand.

The next task was to find the best equipment to increase the pore pressure inside the slope. In the first instance an injection wall was put vertically inside the crest. The idea was that the injection wall would transfer sufficient pressure to the sand, but in practice the friction inside the tubes of the injection wall itself was too large to. Therefore, the injection wall was not able to transfer higher pressure to the sand. An increase of around 0.5 kPa was measured in front of the injection wall.

Another trial was to put an injection tube across the width of the tank and under the toe with a diameter of 25mm. The tube was connected to a pump that could raise the water pressure for at least 440 kPa. The idea was to initiate the liquefaction near the toe of the slope, but there was still too much friction inside the tube that the toe did not liquefy and failure stayed out.

The last option was to increase the pore pressure by using the piping system at the bottom of the tank what is normally used for fluidizing. By installing a pressure chamber to the inlet of the piping system the increase of pore pressure could be better controlled.

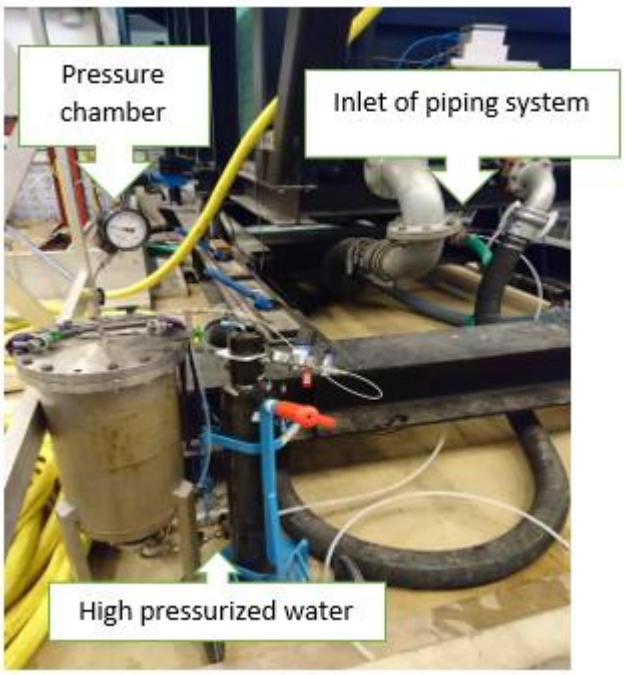

Figure 23: Triggering by using a pressure chamber for water injection to the piping system

For testing the influence of the pressure chamber on the pore pressure in the tank, the time of opening the valve and adapting the backpressure in the pressure chamber were considered. In the end, the backpressure in the pressure chamber was fixed on 3.2 bar (320 kPa) and the time of injection was 20s.

4.3.1.4 Installing the sensors

During fluidization the floating sensors were brought in place in one plane at the middle of the tank, including part of the crest and slope.
From experience the decision was made to put all the sensor in one plane instead of a 3D set up.
The windows of the SL tank were acting as a boundary during liquefaction. Because of that all the sensors were installed in the middle of the tank to measure the liquefaction flow slides with the least influence of the boundaries. An advantage of one plane of sensors, is that is was possible to place the sensors closer to each other and gather more data for 2D pore pressure distribution by interpolation analysis. The sensors at the base are also considered for the interpolation.

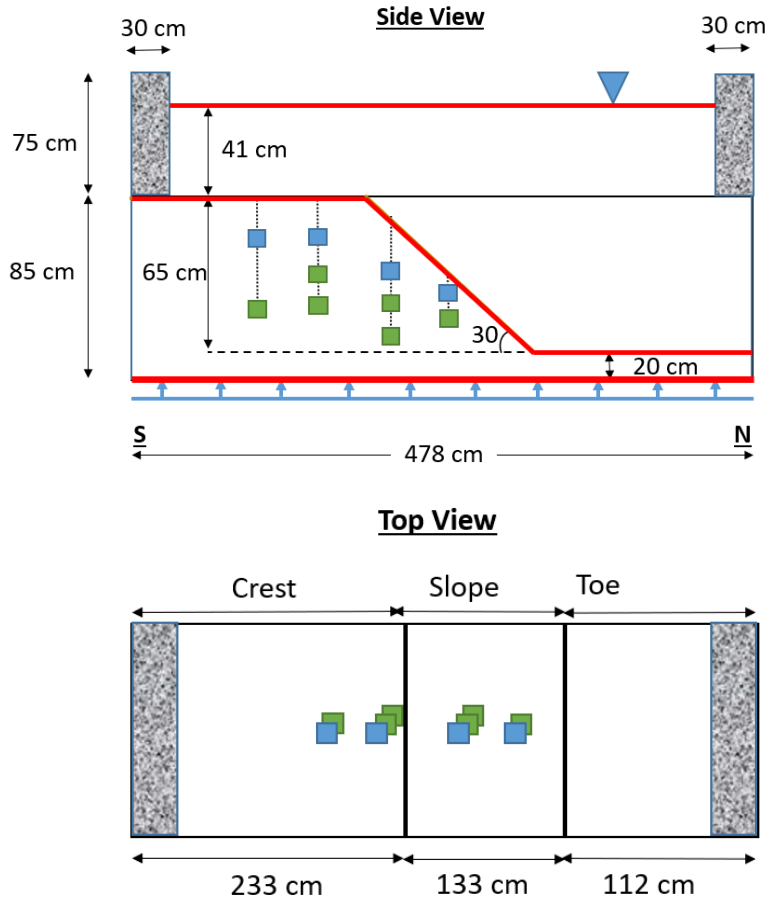

Figure 24: Dimensions of the tank and the location of the sensors. The red lines in the upper graph are the known boundaries conditions

4.3.2 Matlab Interpolation

One of the objectives of the experiment is to simulate the pore pressure distribution in the undrained phase of the static liquefaction. The simulation is done by use of the data from the sensors. The data from the sensors in combinations with the boundary conditions, the values in between are interpolated. The first step was to define the geometry of the sand. A grid or raster was created and the height of the crest, slope and toe were added on the grid. In order to do the interpolation, the geometry of the sand must be stated in a X-Y coordinate system on top of the grid. For example, the start of the crest can be denoted in terms of [X, Y] as [0,85] and the end of the toe as [478,20], in which the crest is 85 cm and the toe 20 cm from the bottom of the tank. The front view of the tank is from left to right or from South to North.

The next step is to add the initial pore pressure values on the grid, that are used for the interpolation. These values are the known hydrostatic boundaries condition beforehand. The known boundary values are: pressure at water level (0 kPa) and the pressure at the crest, slope, toe and base. The pressures are calculated by height of water column above the boundary and multiplied by unit weight of water. These values do not change during the interpolation in the undrained phase.

Subsequently all the sensors must be positioned on the grid with their X and Y coordinates.
The exact positions of the sensors are difficult to define, because they are inside the sand. The horizontal position [X] was estimated based on the location where the wires of the sensors enters the sand. The vertical position [Y} was determined by reading the in-situ pressure from the sensor data at rest and subtract from that the air pressure and derive the height of the sensors in the tank (considering the water column above the sensor as the measured pressure). In appendix it is made clearer. From now, the interpolation can start. For the interpolation the built-in function 'scatteredInterpolant' is used (Mathworks, sd). The known boundary values are treated as scattered point on a grid. The function has as input a vector containing all the coordinates [X,Y] of the boundaries and sensors and a vector containing the corresponding pore pressure values [PP]. The function can be formulated as follows:

[13] $$PP_{Interpolation} = scatteredInterpolant(x, y, PP, 'linear')$$

The method of interpolation is 'linear' what use linear interpolation between the known values.
As expected, the values from the sensors are changing over time and therefore a for loop is made to do the interpolation every time step. The boundary values are fixed, and the sensor data is a function of time. The start of the undrained phase is estimated by looking at the time values where the pore pressure suddenly starts to increase (at the moment of the base injection). The end of the undrained phase is estimated by looking for the time step where the first sensors starts to measure changing acceleration. The last step is to plot the interpolated values over the entire grid and draw an animated plot.

The interpolation is also used for determining the development of the vertical effective stress during the undrained phase. In this case the geometry of the sand is the same as for the pore pressure interpolation, but in each column of the sand, the values for the total vertical stress (kPa) acting in the sand every 1cm of depth (resolution of the grid) is added on the grid. The initial total vertical stress is fixed and during the undrained phase, the two interpolated grids 1) total vertical stress and 2) the pore pressure are subtracted from each other and a new grid is obtained with the vertical effective stress at location [X, Y].

5 Results

5.1 Initial conditions

The initial conditions of the pore pressure distribution are expected to be hydrostatic. The figure below shows the development of the pore pressure in the submerged sand. The water level is measured to be at 126cm above the base (middle) of the tank.

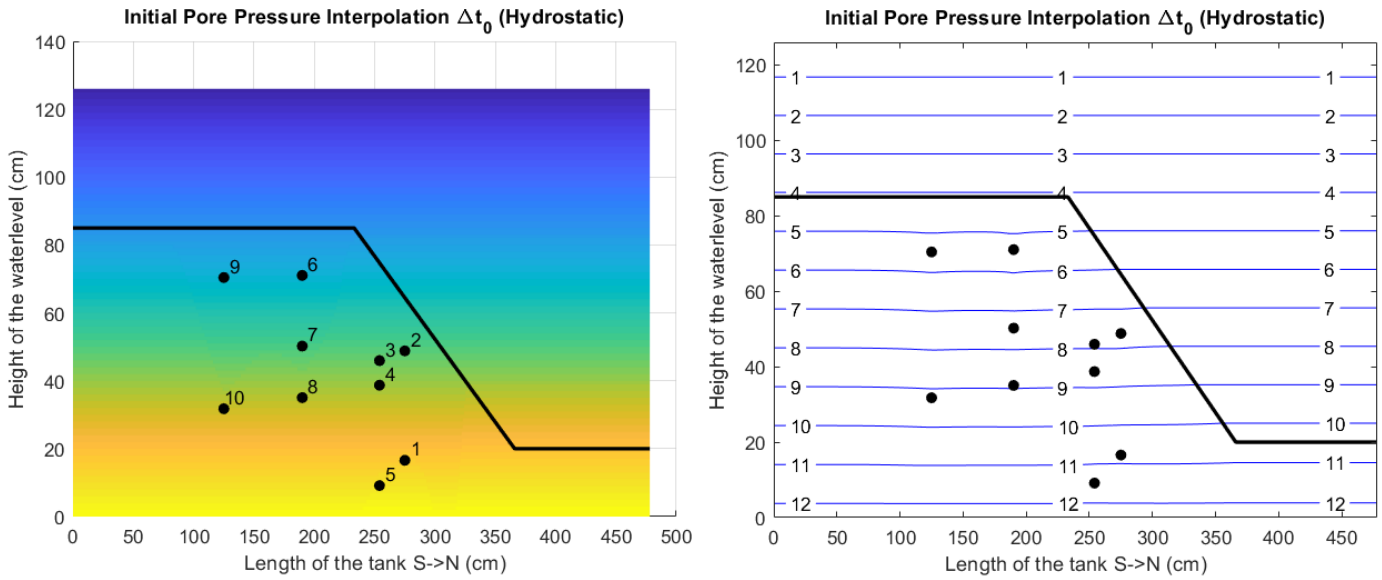

Figure 25: Initial pore pressure distribution displayed by colormap and contour lines (in kPa)

The black dots in Figure 25: Initial pore pressure distribution displayed by colormap and contour lines (in kPa)are the floating sensors in the sand. Five floating sensors are in the slope (1-5) and five floating sensors (6-10) are in the crest. Based on the information given by the sensors, the interpolation is simulated over time. The sensors are inside the sand, so the exact location of the sensors has to be estimated. The location in X-direction (along the length of the tank) is estimated by measuring from the south side of the tank. The position of the sensors in vertical Y-direction (height in the sand) is calculated by reading the initial pore pressure measured by the sensor at rest and then recalculated by subtracting the air pressure from the data. In Appendix 7.2 it is further explained.
There is a small error visible in the contour plot, causing a small bending in the contour lines near the sensors. The error is in a range of 0.1 kPa and probably slipped in by creating the data frame.
The sensors are located at the following positions from S->N:

	Sensor1	**Sensor2**	**Sensor3**	**Sensor4**	**Sensor5**	**Sensor6**	**Sensor7**	**Sensor8**	**Sensor9**	**Sensor 10**
X	285	285	260	260	260	190	190	190	125	125
Y	16.6	48.8	46.0	38.7	9.1	71.0	50.2	35.0	70.4	31.8

Table 1: Locations of the floating sensors

5.2 Definition of undrained phase

The undrained phase can be determined by looking to the graphs of the pore pressures sensors and the accelerometers. As mentioned in the literature study, static liquefaction may occur if the soil is in a certain stress state and brought into a region of instability. When the instability is significant, the sand will deform and liquefaction flow slides are formed. The first stage of liquefaction can be defined as loading under undrained conditions, whereby the water is not allowed to drain out of the submerged sand. The loading is mostly taken by the pore water and results is an increase of the pore water pressure and a decrease in the effective stress. At a certain moment the sand starts to deform and the accelerometers will measure these changes. In Figure 26 for all the sensors the undrained phase is determined by comparing the moment of pore pressure increase at the base (triggering) and the start of changes in acceleration of the sensors. There is a kind of time delay between those two events. The start of acceleration for each sensor is marked by the vertical green line. An important note is that the base triggering last for 10 seconds in total, so what means that is was still triggering after the undrained phase was ended.

1

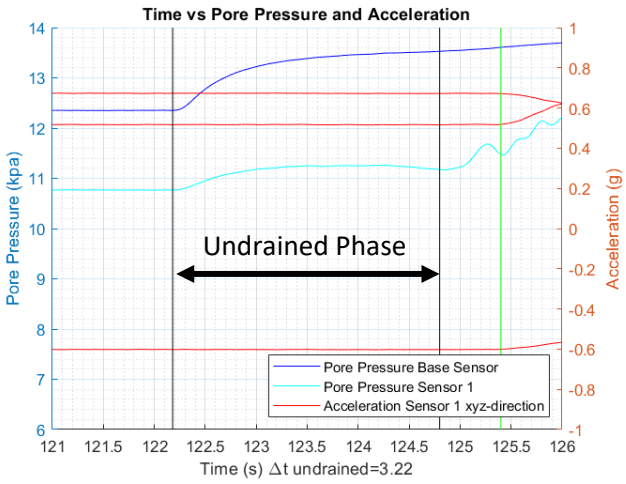

2

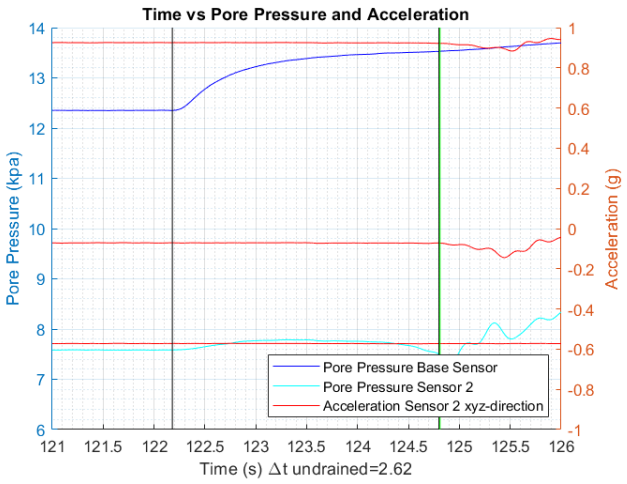

3

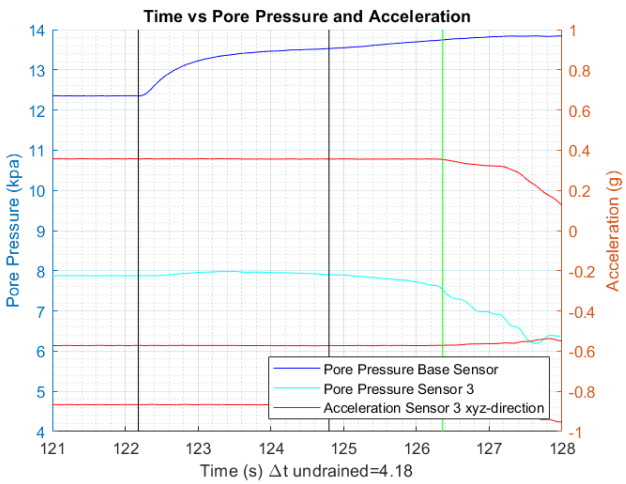

4

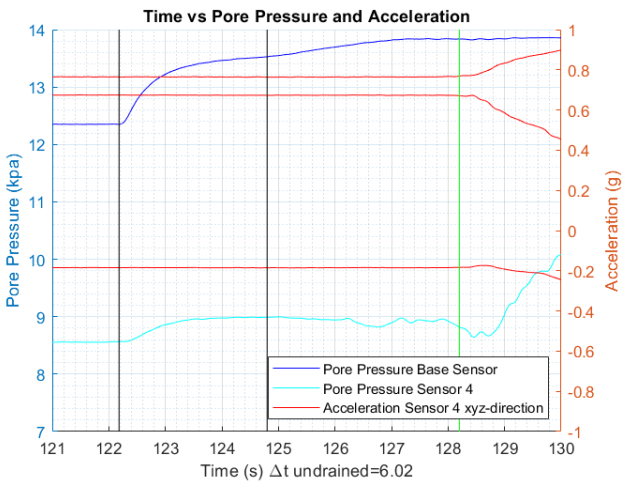

5

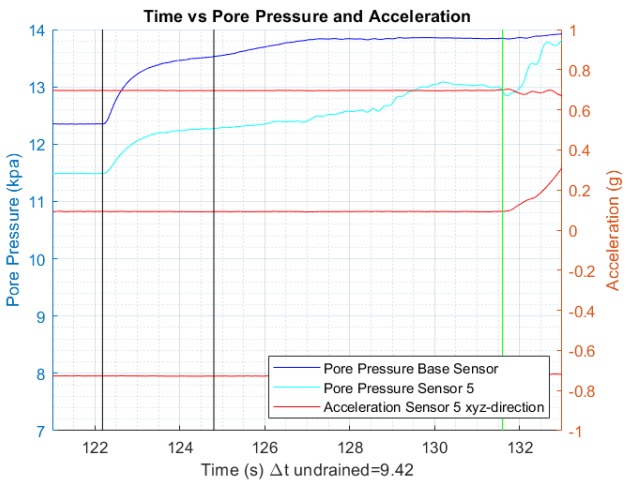

6

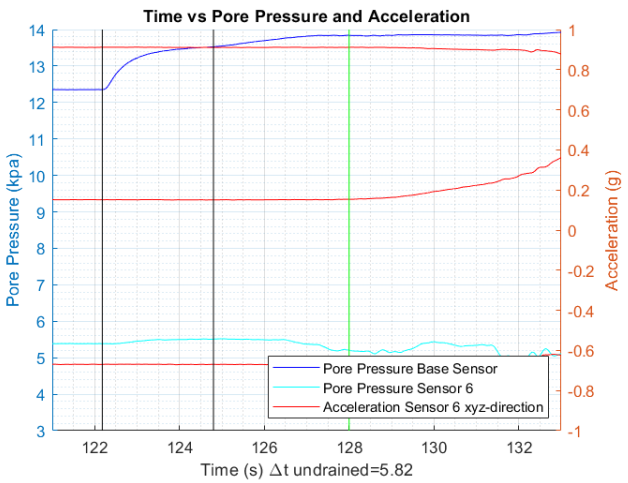

7

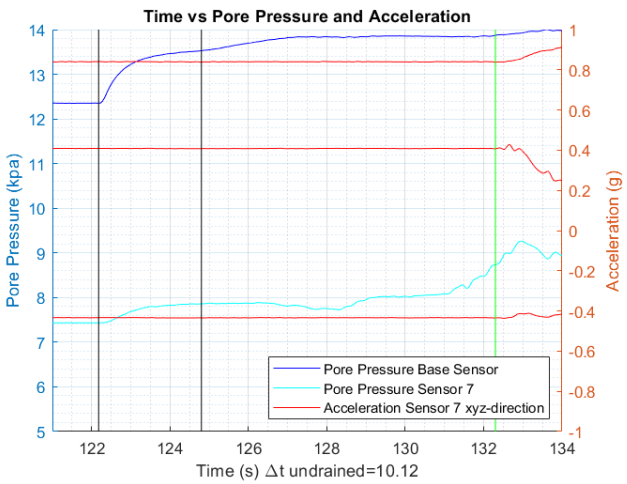

8

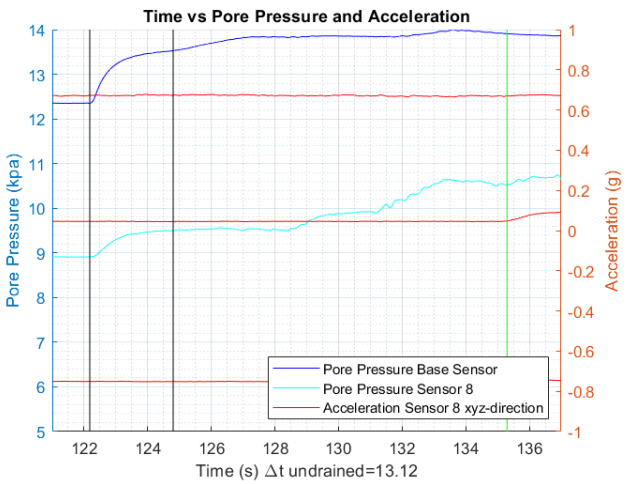

9

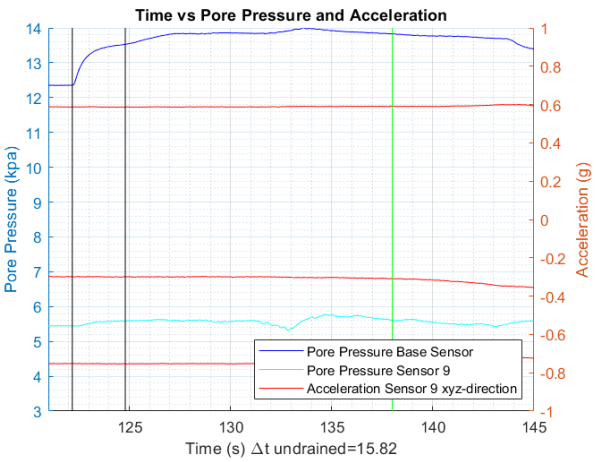

10

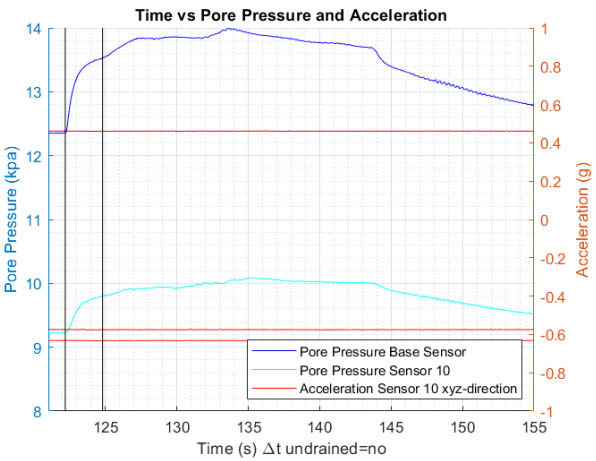

Figure 26: Determining the undrained phase for every sensor and showing their pore pressure development (light blue).

As the plots show, there is not one undrained phase for the entire sand. Most of the sensors show almost directly an increase in pore pressure after base triggering, but the time of deformation can vary widely through the sand. Thus, determining one specific undrained phase is not that clear, but in this experiment the undrained phase is defined as the shortest duration between base triggering and any deformation. The sensor that agrees with this definition is sensor 2. Whereby the undrained phase or time delay appears to be 2.62 seconds. The undrained phase last from 122.18s to 124.8s.

5.3.1 Pore pressure development after base triggering

The pore pressure development of all the sensors together in one plot are shown in Figure 27. The vertical black lines indicate the time interval of the undrained phase.

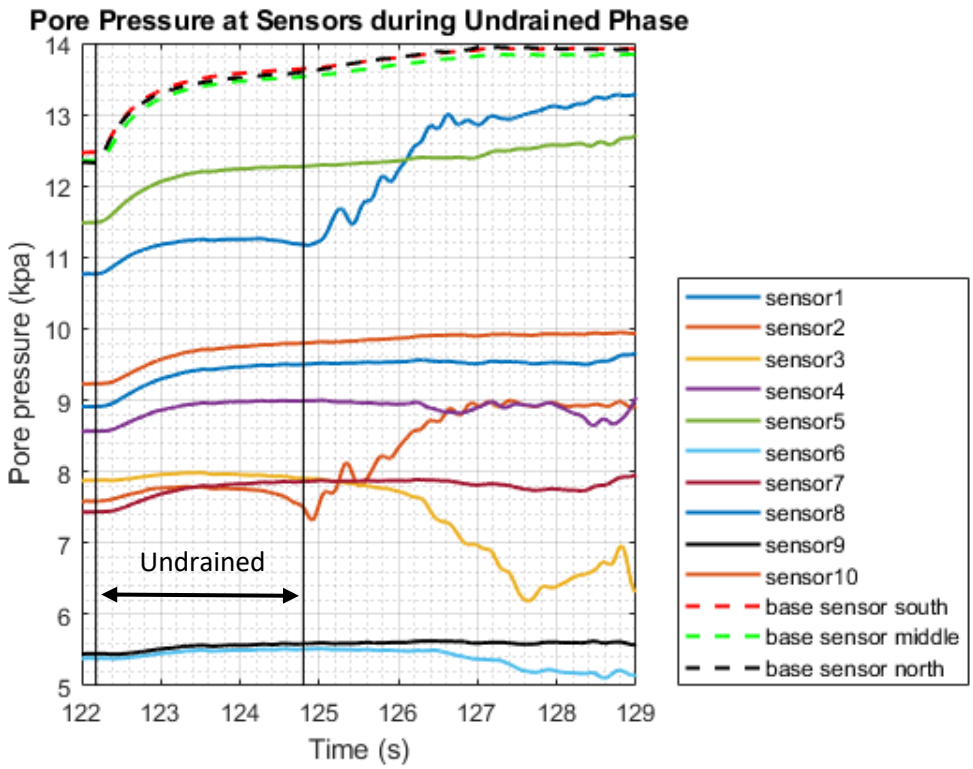

Figure 27: Pore pressures measures by the sensors in the sand over time

One interesting point is that the magnitude of the injection pressure is not distributed directly uniform through the sand. In the undrained phase, the upper most sensors 3,6 and 9 are relative the least influenced by the base triggering. For sensor 6 and 9 is reasonable because the distance between the piping system and the sensors are the largest. On the other hand, sensor 5 shows the largest increment, because this sensor is located as closest to the base of the tank. Another remarkable point is that for sensor 2, the pore pressure at the start of the undrained phase is slightly higher than at the end. This behavior cannot be seen from the pressure development of the other sensors in this same time interval, in which the pressure at the start is lower than the pressure at the end.

Returning to the formulated sub question 2 in section 1.2, a simulation of the pore pressure distribution in the undrained phase can be performed after the MATLAB code is accomplished.
Before triggering, the assumption is made that the entire sand is fully saturated and that hydrostatic conditions are applied, because of the loose configuration and the relatively high hydraulic conductivity in the sand.

5.3.2 Pore pressure distribution after base triggering

The measured pore pressure increment by the sensors can also be displayed by interpolating the values within the geometry of the sand. As mentioned before, the boundary values are already known and fixed during the undrained phase (crest, slope, toe & water). The data from the floating sensors in the sand and the base sensors are also known but are changing over time and used in the interpolation. distribution is stated.

The development of the pore pressure by the use of contour lines is given in the figure below. To compare the pore pressure in relation to the initial pore pressure (hydrostatics), a colormap of the excess pore pressure is also given. The excess pore pressure is obtained by subtracting the initial pore pressure (t=0) from the interpolated pore pressure distribution over time (t = $i\Delta t$).

1

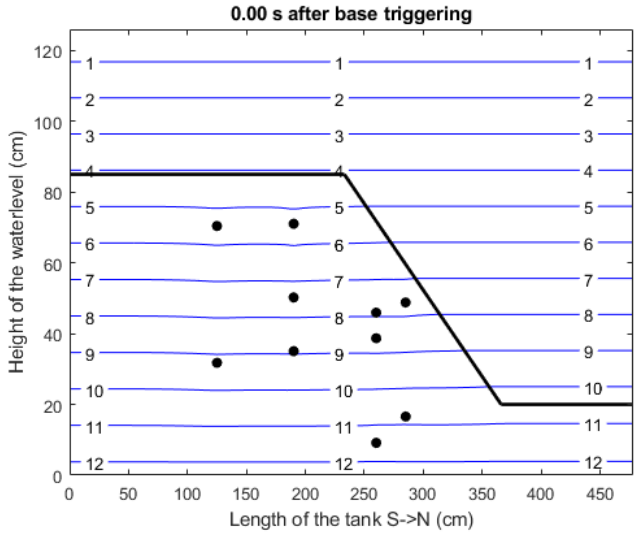

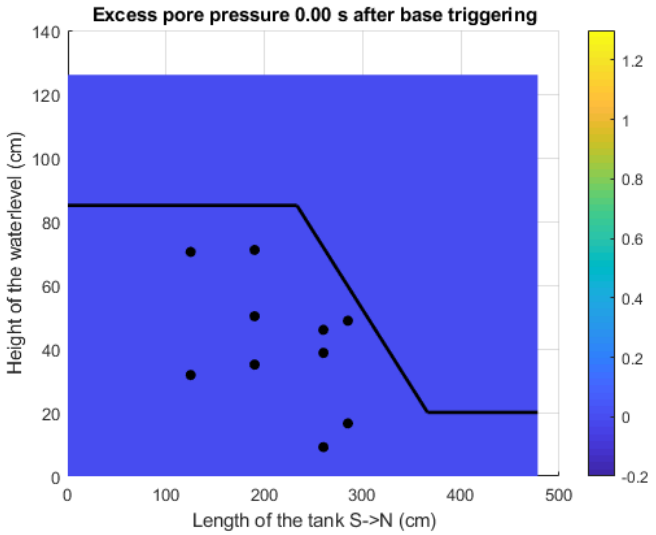

2

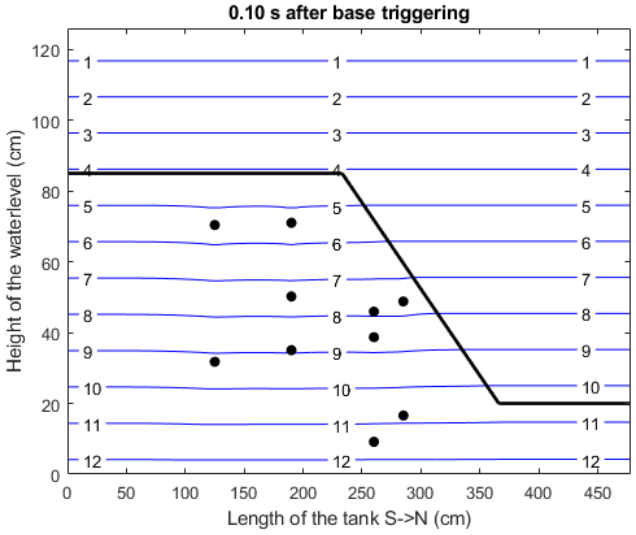

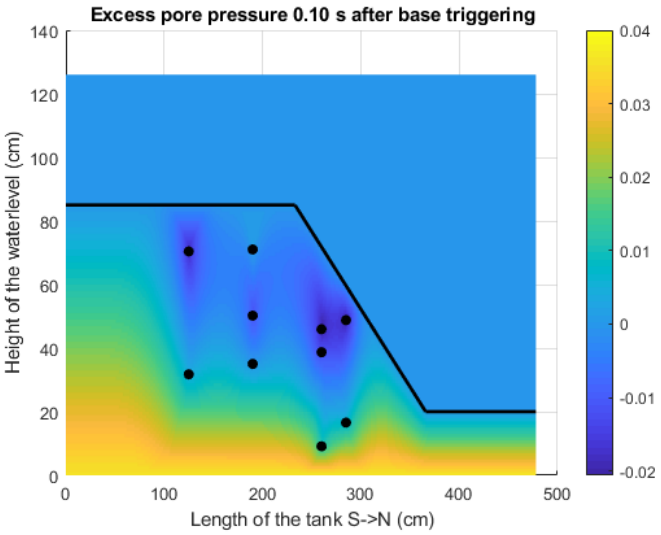

3

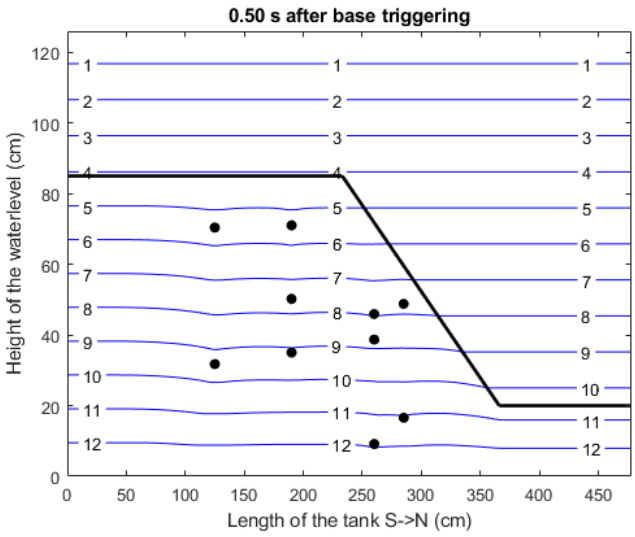
0.50 s after base triggering
Height of the waterlevel (cm)
Length of the tank S->N (cm)

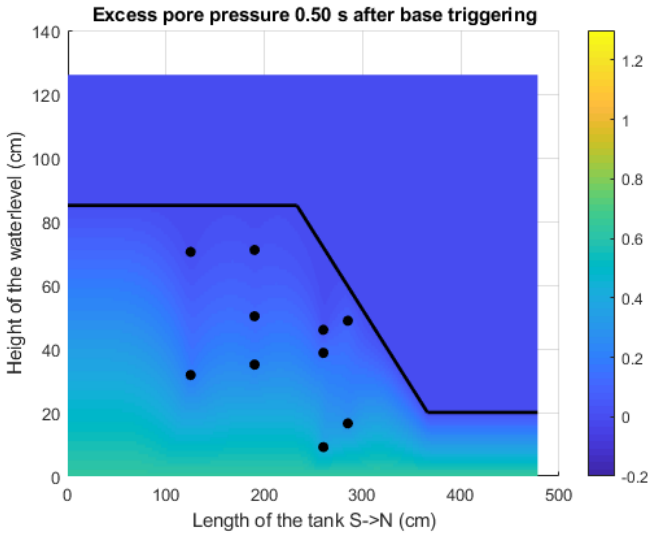
Excess pore pressure 0.50 s after base triggering
Height of the waterlevel (cm)
Length of the tank S->N (cm)

4

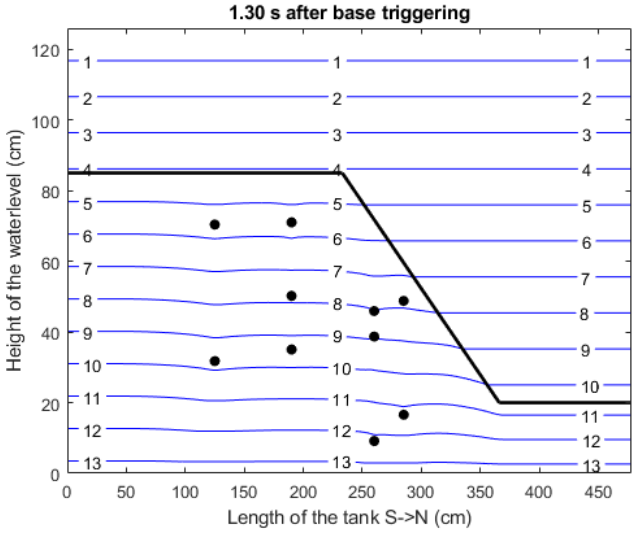
1.30 s after base triggering
Height of the waterlevel (cm)
Length of the tank S->N (cm)

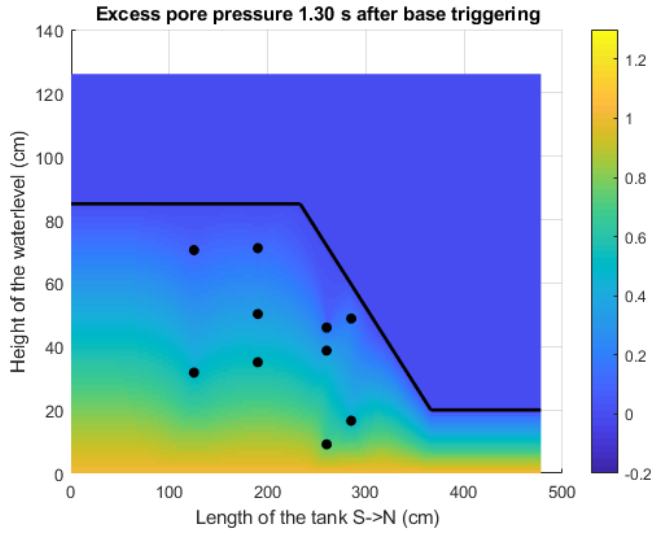
Excess pore pressure 1.30 s after base triggering
Height of the waterlevel (cm)
Length of the tank S->N (cm)

5

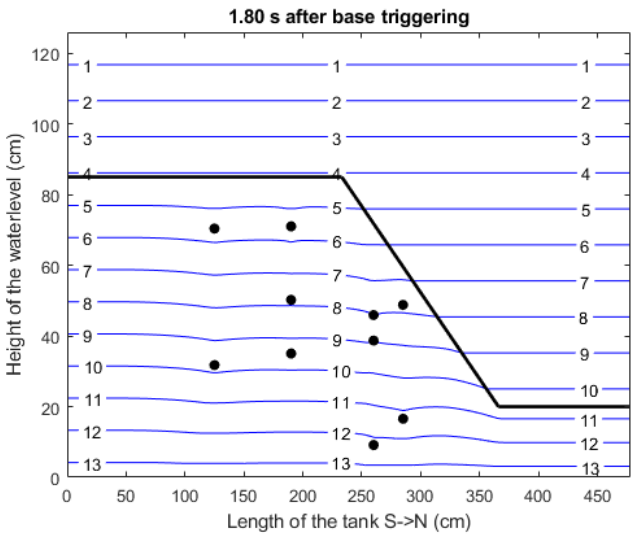
1.80 s after base triggering
Height of the waterlevel (cm)
Length of the tank S->N (cm)

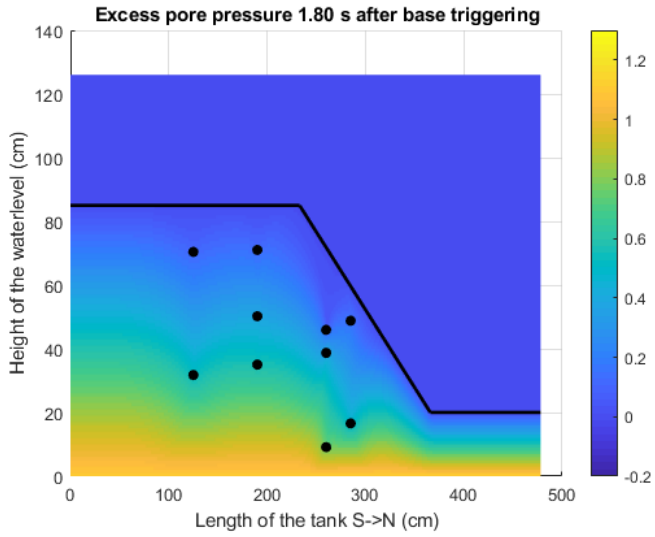
Excess pore pressure 1.80 s after base triggering
Height of the waterlevel (cm)
Length of the tank S->N (cm)

6

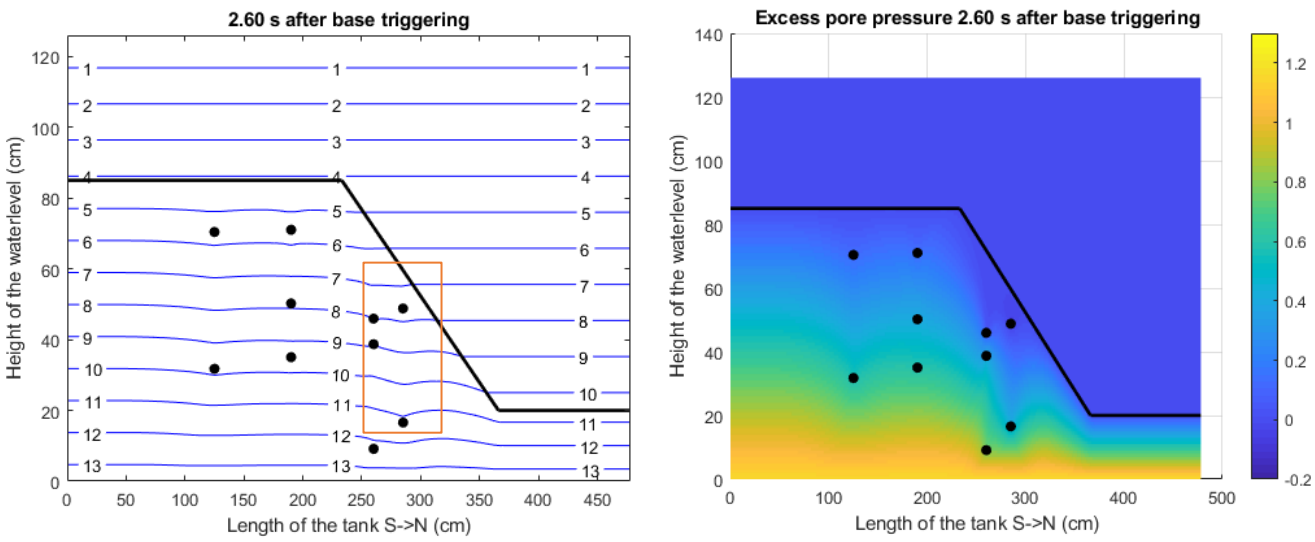

Figure 28: Contour map of pore pressure development (left) and colormap of excess pore pressure (right) during undrained phase

In line with the expectations the pore pressure increases during base injection. As mention before, the base injection last for 10 seconds, so the excess pore pressure will increase more over time than showed above. In Figure 28.2, at 0.10s after start of base injection, there seems to be a negative pressure, probably this is caused by opening the valve from the piping system and the pressure drops for a very short moment. The scale of the legend is adjusted, so it deals with very small values. Furthermore, at t=2.6 seconds, the contour lines under sensor 2 are bended down in comparison with all the other contour lines moving up. When we zoom in at the pore pressure development measured by the sensor 2, this is in accordance with the measured pore pressure development for sensor 2. The pore pressure at the base is increasing while halfway the undrained phase the pore pressure at sensor 2 and 3 (both closest the slope surface) are decreasing.

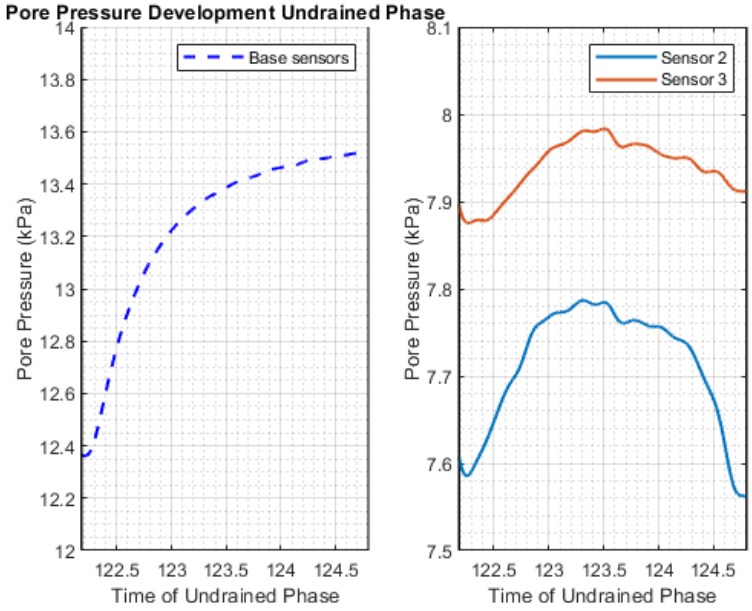

Figure 29: The development of the pore pressure at the base sensor (left) compared with sensor 2 and 3 (right) in the slope

Last point to note, is that the injection from the base does not look to spread out uniformly, the most likely reason is the error in linear interpolation or that the outflow from the piping system varies at the base (least likely).

5.3.3 Vertical effective stress development in undrained phase

Regarding the last sub question, the focus in this part is the development of the vertical effective stress during the undrained phase.
For obtaining the vertical effective stress, the total stress has to be calculated first.
The total vertical stress is calculated by using the saturated unit weight of the sand. From the water level to the bottom of the tank, the total stress is calculated every 1cm in depth. The following formula is used, assuming fully saturation.

[14] $$\gamma_{sat} = \frac{(G+e)*\gamma_w}{1+e}$$

In which *G* is the specific gravity (2.67) and *e* the current void ratio (0.874)
The saturated unit weight becomes 0.185 kPa per cm depth.

The figure below shows the total vertical stress in the sand, starting from the water level.

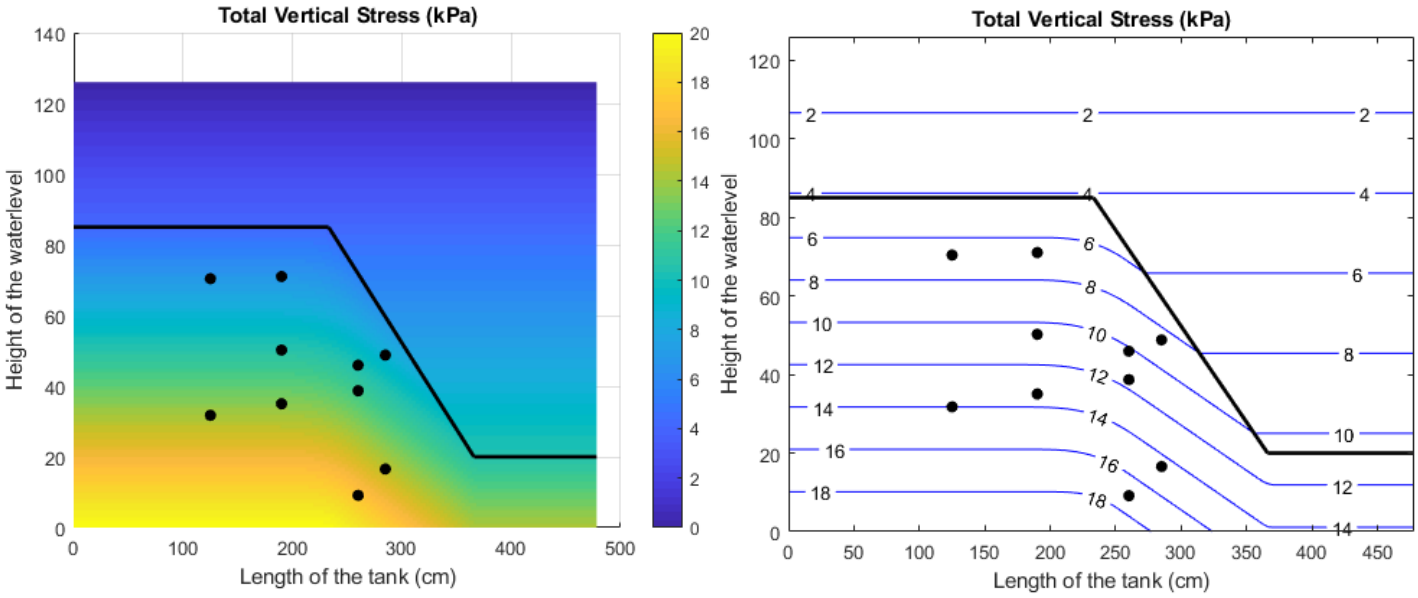

Figure 30: A colourmap of the total vertical stress (right) and a contour map (left) in kPa

The next step is to calculate the vertical effective stress by subtracting the pore pressure distribution at time t_i from the vertical total stress in the sand. In the figure below the vertical effective stress is shown at times 0,1.3 and 2.5 seconds.

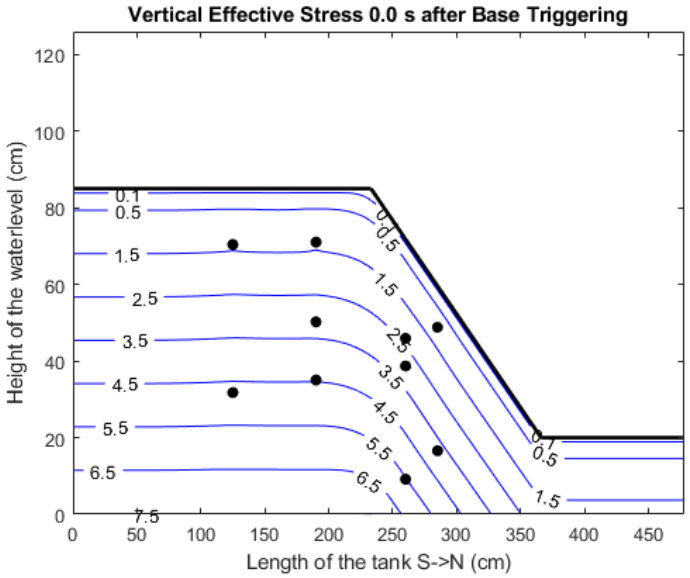
Vertical Effective Stress 0.0 s after Base Triggering
Height of the waterlevel (cm)
Length of the tank S->N (cm)
0.1
0.5
1.5
2.5
3.5
4.5
5.5
6.5
7.5

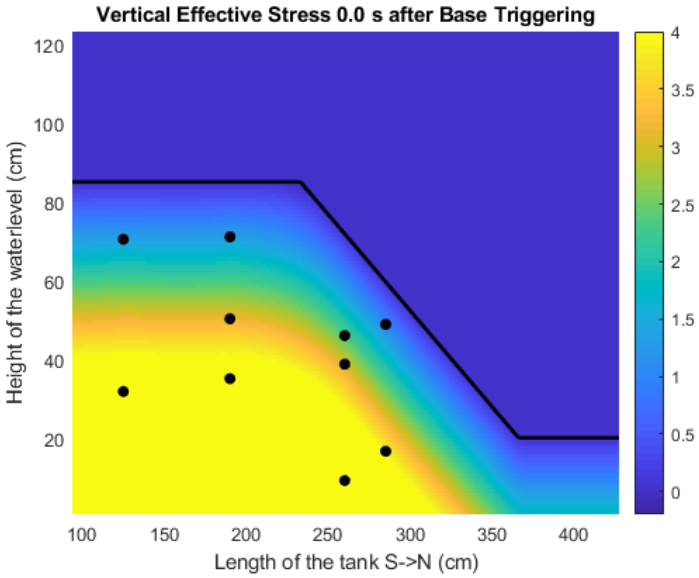
Vertical Effective Stress 0.0 s after Base Triggering
Height of the waterlevel (cm)
Length of the tank S->N (cm)

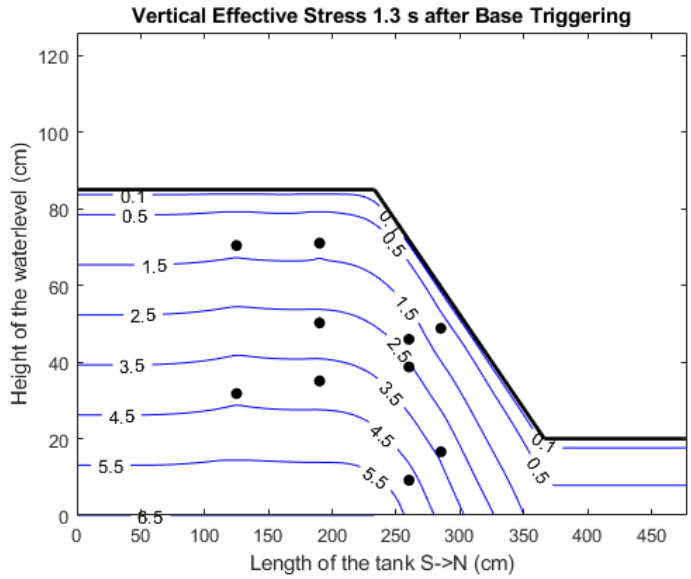
Vertical Effective Stress 1.3 s after Base Triggering
Height of the waterlevel (cm)
Length of the tank S->N (cm)
0.1
0.5
1.5
2.5
3.5
4.5
5.5
6.5

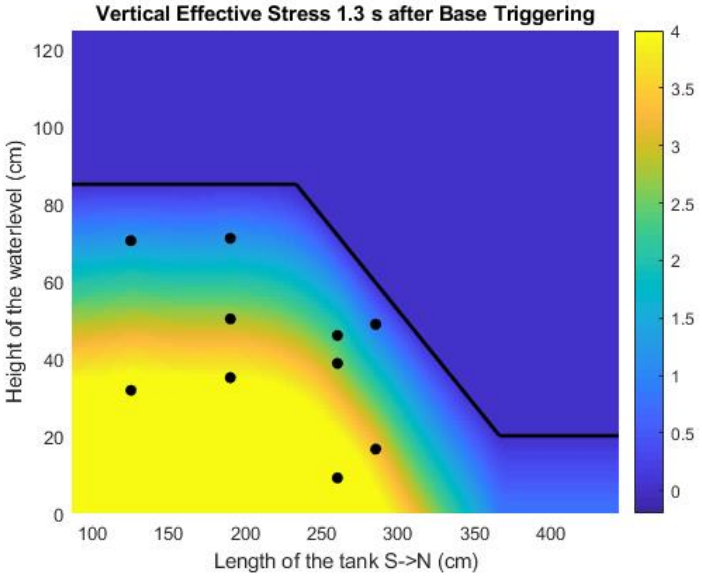
Vertical Effective Stress 1.3 s after Base Triggering
Height of the waterlevel (cm)
Length of the tank S->N (cm)

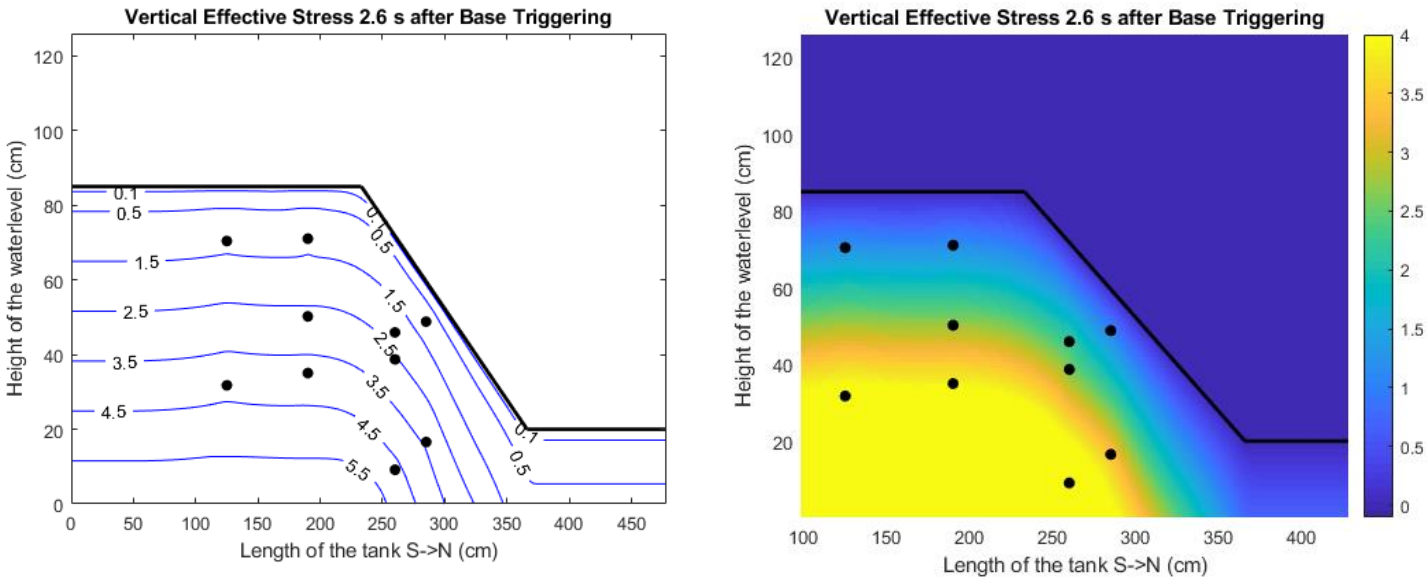

Figure 31: Contour plot of vertical effective stress (left) and colormap of vertical effective stress (right)

Figure 311 Figure 31: Contour plot of vertical effective stress (left) and colormap of vertical effective stress (right)shows that there is a slight reduce in vertical effective stress halfway the slop and in the toe. The contour plot makes it clearer that in the toe the largest decrease in vertical stress has taken place. That is reasonable, because the total vertical stress is already the lowest and base injection reduces the vertical effective stress fast. The static liquefaction induced flow slides are formed in the slope, because on a small scale the sand skeleton is tilted with a different orientation of the principal stresses and shear forces.

5.4 Partially drained and undrained phase

From the previous section about the pore pressure distribution during the undrained phase, the changes were not that significant to draw hard conclusions. To make the pore pressure distribution a bit more interesting, we extend the undrained phase a few seconds till 4.52s time delay. In Figure 32 the extended part stops at 126.7 seconds from base triggering.

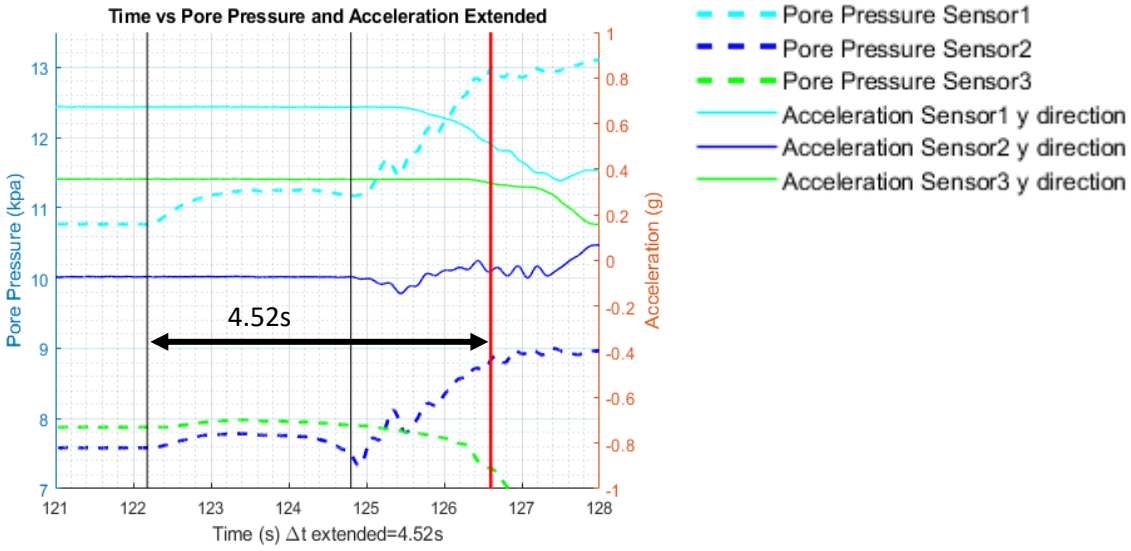

Figure 32: Time delay extended for pore pressure sensor 1,2&3 and acceleration in y directions

From Figure 32, the accelerometers detect small movements of the sensors in this extended time interval. So actually, the position of sensor 1,2 and 3 will changes of time. But for simplicity we keep the positions fixed. In the plots below the excess pore pressures and the vertical effective stress are shown.

1

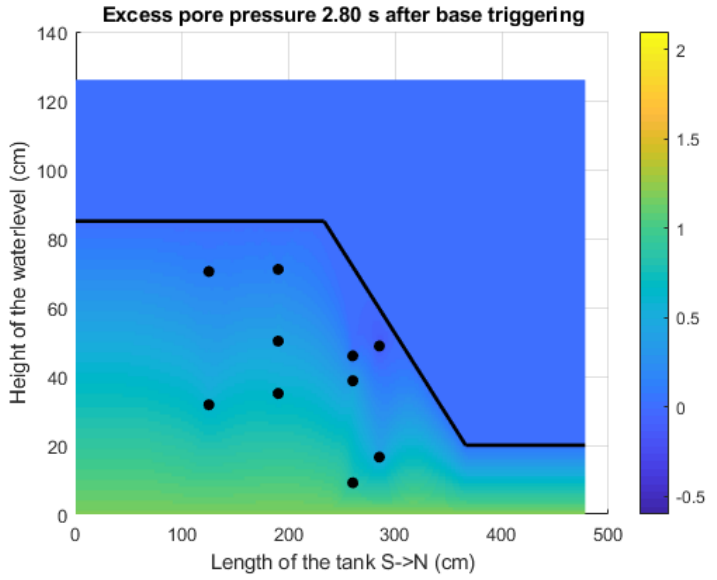

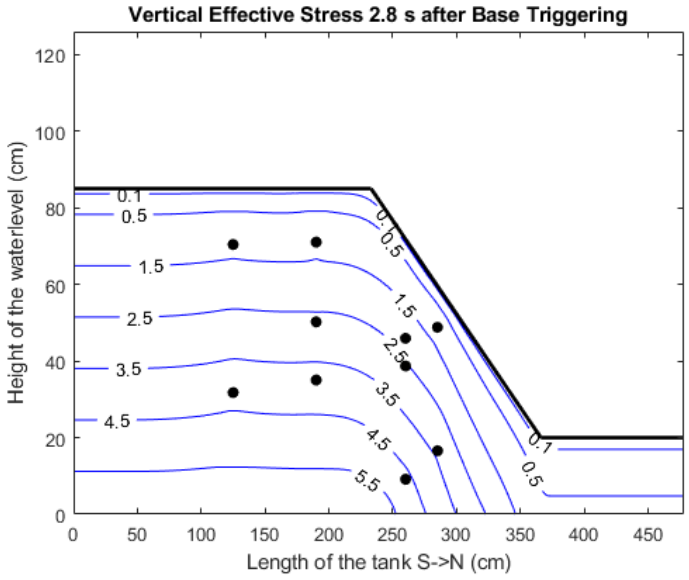

2

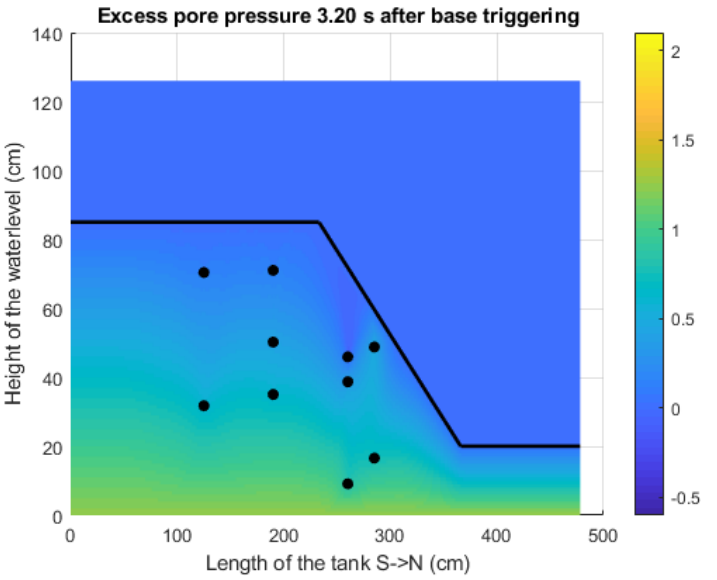

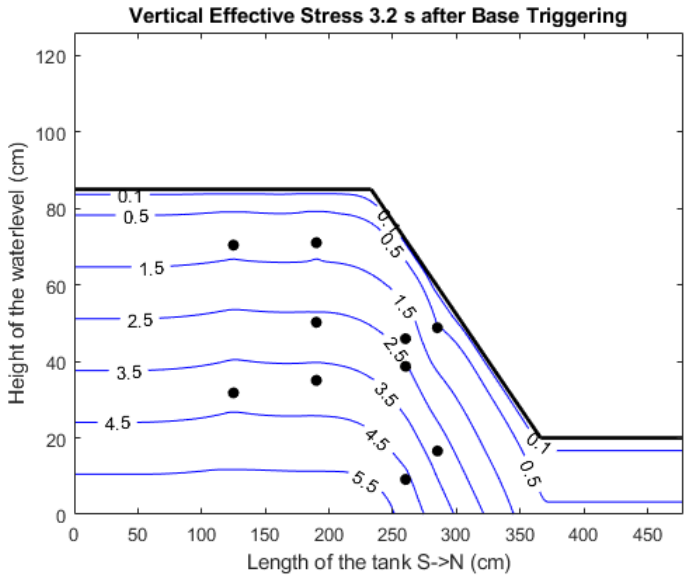

3

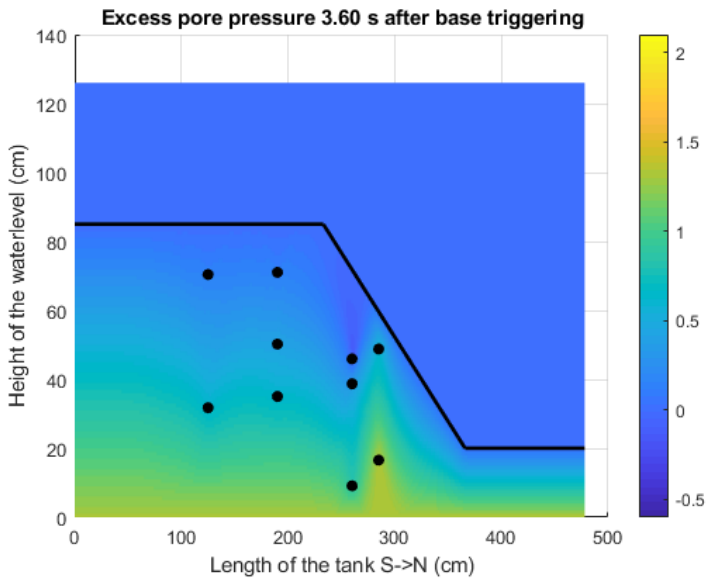
Excess pore pressure 3.60 s after base triggering
Height of the waterlevel (cm)
Length of the tank S->N (cm)

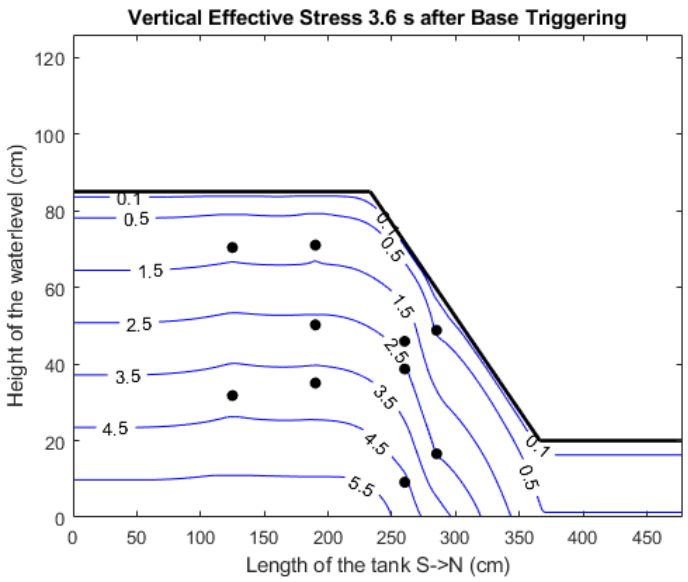
Vertical Effective Stress 3.6 s after Base Triggering
Height of the waterlevel (cm)
Length of the tank S->N (cm)
0.1
0.5
1.5
2.5
3.5
4.5
5.5

4

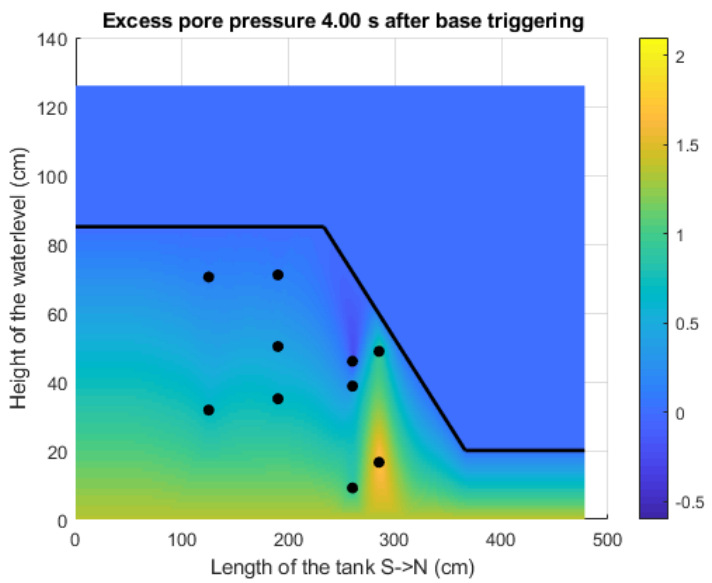
Excess pore pressure 4.00 s after base triggering
Height of the waterlevel (cm)
Length of the tank S->N (cm)

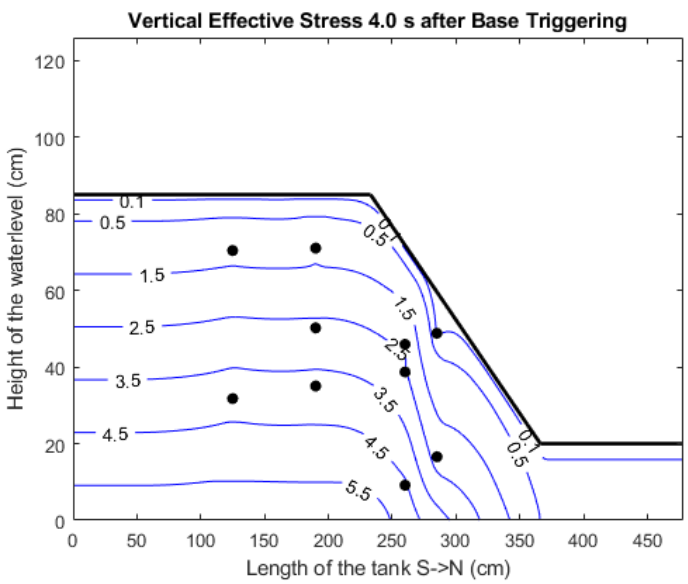
Vertical Effective Stress 4.0 s after Base Triggering
Height of the waterlevel (cm)
Length of the tank S->N (cm)
0.1
0.5
1.5
2.5
3.5
4.5
5.5

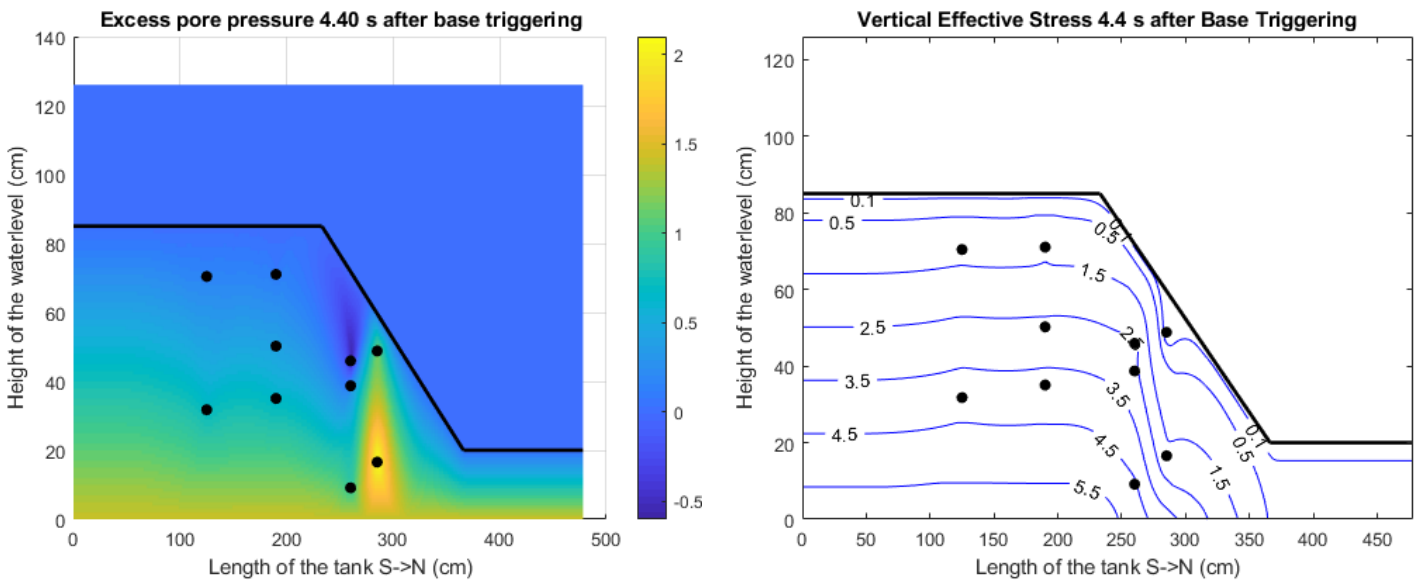

Figure 33: Excess pore pressure (left) and vertical effective stress (right)

In Figure 33 it can be seen that the contour lines (equal pressure lines) with low effective stress enter the sand deeper through the sand over time. From Figure 33.4 and Figure 33.5 it seems that in a short moment very low effective stress contour lines suddenly intrude into the sand and brings the zone around sensor 2 in instability and flow slides are formed. It looks like that the instability is initiated in the slope instead of the toe, but there are no sensors in the toe, so that conclusion cannot be directly verified.

5.5 Recording of the flow slides

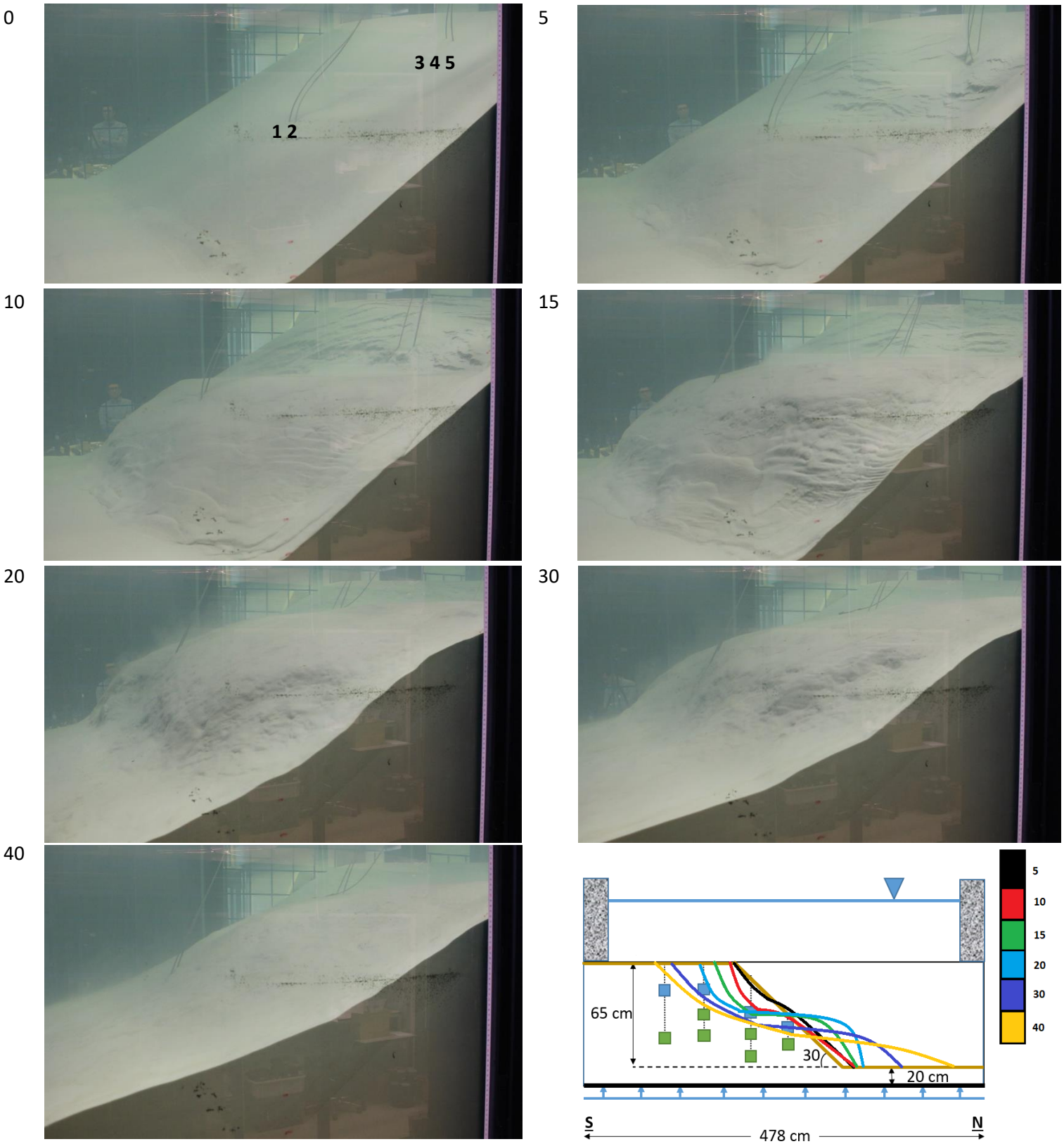

Figure 34: Video fragments of the flow slides from 0 to 40 seconds (sensors 1tm5) and a schematic view of the shape of the slope over time

In the video fragments from Figure 34 it can be seen that the higher part of the slope (at wire with sensor 3,4 & 5) collapses and that the lower part of the slope expands in the first seconds. From 10 second till 30 seconds it looks that halfway the slope a temporary bench is formed. The sand looks quite dense in the beginning and retrogressive flow slides could be visible.

6 Conclusion

As stated in the research questions, the experiment was carried out to gain insights in the concept about the pore pressure distribution during undrained loading of the sand after 20 seconds of triggering.
The triggering mechanism that was used in the experiment was water injection from the base of the tank by use of a pressure chamber.
The undrained phase of the static liquefaction was determined by looking at the start of the pore pressure increment at the base sensor and the moment of the first acceleration measured by one the floating sensors. This time delay was used as indication for the undrained phase.
From the data of the all the floating sensors it can be seen that after base injection the sand does not measure the same magnitude of pore pressure increment, or excess pore pressure, throughout sand.
Another result was that during water injection for 20 seconds, the pore pressure measured by the base sensor were continuously increasing over time, but the sensors closest to the sloping surface (2 & 3) measured halfway the undrained phase a decrease in pore pressure (Figure 29). The quantity of the recorded excess pore pressures and their rate of dissipation is linked to the distance of the sensors from the pressure source and the drainage path (distance to the sand surface). The sudden decrease of pore pressure was followed by change in acceleration of the sensor 2 and the static liquefaction induced flow slides were initiated. The contour plot and colormaps of the vertical effective stress under undrained conditions show that the line of equal effective stress became steeper in the slope than in the initial stage before triggering. In the case that the time delay was extended, the contour plot from Figure 33 shows a large drop in effective stress and a large increase in excess pore pressure around sensor 2 and 3. The effective stress contour lines become steeper and reveals a clear drop of the effective stress at the toe of the slope (Figure 31 and Figure 33Figure 33: Excess pore pressure (left) and vertical effective stress (right), and in combination with large shear forces, the deformation of the sand is significant and flow slides are formed. Besides that, from the recordings it can be seen that the sand collapses at the location between sensor 2 and 3 and is followed by static liquefaction induced flow slides.

7 Recommendations

The results from the pore pressure interpolation can be used as a simplified interpretation for the distribution of the base injection in the undrained phase. The produced data can be improved by using more advanced interpolation methods considering the linear interpolation approach used in this study. In the linearly interpolated pore pressure data, further away from the sensors or boundaries, the interpolation may be less accurate.

Additionally, since the sensors were installed inside the sand layer, there might be possible errors in determination of the exact location of the sensors. This might be resulted by the complex sedimentation process which governs the final location of the sensors after fluidization (sample preparation). In the initial calculation stage, it was assumed that all of the sensors are located at the same 2D plane. However, in reality sensors were moved out of the plane due to shape and stiffness of the data cable attached to them. Furthermore, during dredging the slope, there were some liquefaction flow slides that could change the state of the sand (e.g. density and void ratio) before any triggering was applied.

Overall interpolation could give some good insight into the pore pressure distribution in the undrained phase but is also subjected to some uncertainties related to input of the interpolating function, what automatically brings errors to the results.

8 References

de Groot, M., Lindenberg, J., Mastbergen, D., & van den Ham, G. (2012). *Large scale sand liquefaction flow slides tests revisited.* Delft: Deltares.

Dinoloket. (n.d.). *Ondergrondmodellen*. Retrieved from Dinoloket: https://www.dinoloket.nl/ondergrondmodellen

Dong, Q., Xu, C., Cai, Y., Juang, H., F.ASCE, Wang, J., . . . Gu, C. (2015). *Drained Instability in Loose Granular Material.* American Society of Civil Engineers. International Jounral of Geomechanics.

Eelkema, M. (2013). *Eastern Scheldt Inlet Morphodynamics.* Haveka.

Hoque, M., Ansary, M., & Yasin, S. (2017). *Effects of Relative Density and Effective Confining Pressure on Liquefaction Resistance of Sands.* Deparment of Civil Engineering. Seoul: Bangladesh University of Engineering and Technology.

Huisman, B., & Luijendrijk, A. (2009). *Sand demand of the Eastern Scheldt .* Deltares. Deltares.

Lade, P., & Yamamuro, J. (1992). Static instability and liquefaction of loose fine sandy slopes. *Journal of Geotechnical Engineering 118 (1)*, 51-71.

Lade, P., & Yamamuro, J. (1997). Effects of non-plastic fines on static liquefaction of sands. *Canadian Geotechnical Journal, 34(6)*, 918-928.

Lade, P., & Yamamuro, J. (2009). *Evaluation of static liquefaction potential of silty sand slopes.* NRC Research Press Web.

Lade, P., & Yamamuro, J. (2011). Evaluation of static liquefaction potential of silty sand slopes. *Canadian Geotechnical Journal*, 252.

Maghsoudloo, A., Askarinejad, A., de Jager, R., Molenkamp, F., & Hicks, M. (n.d.). *Experimental investigation of pore pressure and acceleration development in static liquefaction induced failure in submerged slopes.* Delft University of Technology, Section of Geo-Engineering.

Mathworks. (n.d.). *Scattered Interpolant*. Retrieved december 2018, 15, from https://nl.mathworks.com/help/matlab/ref/scatteredinterpolant.html

Owen, G., & Moretti, M. (2011). *Identifying triggers for liquefaction-induced soft sediment deformation in sands.* Swansea University, Department of Geography. Swansea : Elsevier B.V.

Peters, J. (1991). *Discussion of instability of granular materials with nonassociated flow.* Journal of Engineering Mechanics.

Silvis, F., & de Groot, M. (1995). *Flow slides in the Netherlands: experience and engineering practice.* Can. Geotech.

Sladen, J., D'Hollander, R., Krahn, J., & Mitchell, D. (1985). *Back analysis of the Nerlek berm liquefaction slides.* Canadian Geotechnical Journal.

Terzaghi, K., Peck, R., & Mesri, G. (1996). *Soil Mechanics in Engineering Practise* (Vol. Third Edition Wiley). New York.

Tsuchida, H. (1970). *Prediction and countermeasure against the liquefaction in sand deposits. .*

van der Krogt, M., van den Ham, G., & Kok, M. (2015). Safety Assessment Method of Flood Defences for Flow Sliding. *Geotechnical Safety and Risk V*, 522.

9 Appendix

9.1 Matlab code sensor data

```
%% Reading the DEMO output data files
%This code is witten to read an analyze the "Arash23052017_Trial.bin".
clc
fid = fopen('20190118 The Big Failure Test2','r');
NColumns = 71; % thats the number of columns
% Sample0: TimeStampL, TimeStampH, DataChannel0, DataChannel1, ...,
dataChannle67, Pos
% >>> 71 columns for current format of data (March 2017)
%Data = fread(fileID, sizeA, precision, skip, machineformat)
Data = fread(fid,inf,'single',0,'l');
fclose(fid);
%%
% Remove first four numbers (32 bytes)which shows the time reference
% Data-edit is the complete data set without the fisrt 32 bit
Data_edit = Data(5:end);
Data_edit = Data_edit';

% Reshape the array to the matrix of data and channels
start_undrained = 122.15*1000;
end_undrained = 125.40*1000;
start_plot = 120*1000;
end_plot = 200*1000;
start_acc = 1.2335*10e5;
end_acc = 1.245*10e5;
Data_mod = reshape (Data_edit,NColumns,[]);
Data_final= Data_mod';
%% Reducing size of data
Data_final= Data_final(start_undrained:end_undrained,:);

%% Filter design
% Butterworth filter
    fc = 5;              %Cut off frequency
    fs = 1000;           %Sampling rate in Hz
    ts = 1/fs;           %sampling time in sec
    [b,a] = butter(6, fc/(fs/2),'low'); % [B,A] = butter(N,Wn,'low')
designs a lowpass filter where N is the order and Wn is the cut off
freq.(0.0 < Wn < 1.0) and Wn=target freq/fs/2;
%% Making a dataset for all the channels. Starting from channel 0, what is
from column 3 in Data_fil
size_data_fil = size(Data_final);
channels = zeros(size_data_fil(1),size_data_fil(2)-3);
air = 99.0; % air pressure, weather. Has to be subtracted from sensor
measurements
g = 9.81;
time = Data_final(:,1)./10e5;
dt=250; %every 0.25s the data is used
time1 = time(1:dt:end);
for ii = 1:size_data_fil(2)-2
channels(:,ii) = filtfilt(b,a,Data_final(:,ii+2));
end



%%
for ii = 1:size_data_fil(2)-2
Data_fil(:,ii+2) = filtfilt(b,a,Data_final(:,ii+2));
channels(:,ii) = Data_fil(:,ii+2);
end
```

```
%% All the acceleration sensors with xyz columns (pairs of 3)
num_accxyz_col = [1 2 3, 5 6 7, 9 10 11, 13 14 15, 17 18 19, 21 22 23, 25
26 27,...
    29 30 31,33 34 35,37 38 39];
acc_sensors = zeros(size_data_fil(1),length(num_accxyz_col));
for jj = 1:length(num_accxyz_col);
    acc_sensors(:,jj) = channels(:,num_accxyz_col(jj));
end
%% All the pore pressure sensors (floating and fixed to tank)
num_pp_sensors_col = [4 8 12 16 20 24 28 32 36 40 51 52 53 54 55 56 57]; %
all floating pore pressure sensors
PP_sensors = zeros(size_data_fil(1),length(num_pp_sensors_col));
for kk = 1:length(num_pp_sensors_col);
    PP_sensors(:,kk) = channels(:,num_pp_sensors_col(:,kk));
end

%% Finding the xyz linear acceleration of every sensor,...
% by subtracting the component of gravity of every component.
% first find all the angles to the vertical of every component
air = 101.83; % air pressure, weather. Has to be subtracted from pore
pressure value
g = 9.81;
calibration_base = 2.1074; % because the sensors at the base are around 20
cm below the sand,...
% we have to correct for those and use the pressure at the bottom of the
% sand instead of bottom of the tank. (at the bottom of the sand the
% pressure is slightly lower)
%% Floating sensor 1 tm 10
fl_sensor1_accx = acc_sensors(1:dt:end,1);
fl_sensor1_accy = acc_sensors(1:dt:end,2);
fl_sensor1_accz = acc_sensors(1:dt:end,3);
fl_sensor1_p = PP_sensors(1:dt:end,1)-air;

fl_sensor2_accx = acc_sensors(:,5);
fl_sensor2_accy = acc_sensors(:,6);
fl_sensor2_accz = acc_sensors(:,7);
fl_sensor2_p = PP_sensors(1:dt:end,2)-air;

fl_sensor3_accx = acc_sensors(:,7);
fl_sensor3_accy = acc_sensors(:,8);
fl_sensor3_accz = acc_sensors(:,9);
fl_sensor3_p = PP_sensors(1:dt:end,3)-air;

fl_sensor4_accx = acc_sensors(:,10);
fl_sensor4_accy = acc_sensors(:,11);
fl_sensor4_accz = acc_sensors(:,12);
fl_sensor4_p = PP_sensors(1:dt:end,4)-air;

fl_sensor5_accx = acc_sensors(:,13);
fl_sensor5_accy = acc_sensors(:,14);
fl_sensor5_accz = acc_sensors(:,15);
fl_sensor5_p = PP_sensors(1:dt:end,5)-air;

fl_sensor6_accx = acc_sensors(:,16);
fl_sensor6_accy = acc_sensors(:,17);
fl_sensor6_accz = acc_sensors(:,18);
fl_sensor6_p = PP_sensors(1:dt:end,6)-air;

fl_sensor7_accx = acc_sensors(:,19);
fl_sensor7_accy = acc_sensors(:,20);
fl_sensor7_accz = acc_sensors(:,21);
```

```
fl_sensor7_p = PP_sensors(1:dt:end,7)-air;

fl_sensor8_accx = acc_sensors(:,22);
fl_sensor8_accy = acc_sensors(:,23);
fl_sensor8_accz = acc_sensors(:,24);
fl_sensor8_p = PP_sensors(1:dt:end,8)-air;

fl_sensor9_accx = acc_sensors(:,25);
fl_sensor9_accy = acc_sensors(:,26);
fl_sensor9_accz = acc_sensors(:,27);
fl_sensor9_p = PP_sensors(1:dt:end,9)-air;

fl_sensor10_accx = acc_sensors(:,28);
fl_sensor10_accy = acc_sensors(:,29);
fl_sensor10_accz = acc_sensors(:,30);
fl_sensor10_p = PP_sensors(1:dt:end,10)-air;

base_sensor_n = PP_sensors(1:dt:end,11)-calibration_base;
base_sensor_m = PP_sensors(1:dt:end,12)-calibration_base;
base_sensor_s = PP_sensors(1:dt:end,13)-calibration_base;

wall_sensor_s1 = PP_sensors(1:dt:end,14); % 50cm from bottom
wall_sensor_n2 = PP_sensors(1:dt:end,15); % 23 cm
wall_sensor_s1 = PP_sensors(1:dt:end,16); % 50 cm
wall_sensor_s2 = PP_sensors(1:dt:end,17); % 50 cm
%% All the measured pore pressure by the sensors (filtered data)
figure(1)

plot(time1,fl_sensor1_p,'LineWidth',1.5)
hold on
plot(time1,fl_sensor2_p,'LineWidth',1.5)
hold on
plot(time1,fl_sensor3_p,'LineWidth',1.5)
hold on
plot(time1,fl_sensor4_p,'LineWidth',1.5)
hold on
plot(time1,fl_sensor5_p,'LineWidth',1.5)
hold on
plot(time1,fl_sensor6_p,'LineWidth',1.5)
hold on
plot(time1,fl_sensor7_p,'LineWidth',1.5)
hold on
plot(time1,fl_sensor8_p,'LineWidth',1.5)
hold on
plot(time1,fl_sensor9_p,'k','LineWidth',1.5)
hold on
plot(time1,fl_sensor10_p,'LineWidth',1.5)
hold on
plot(time1,base_sensor_s,'--r','LineWidth',1.5)
hold on
plot(time1,base_sensor_m,'--g','LineWidth',1.5)
hold on
plot(time1,base_sensor_n,'--k','LineWidth',1.5)
hold on
grid on
grid minor
xlim([start_undrained/1000 end_undrained/1000]);
ylim([4 17]);
title('Pore Pressure at Sensors during Undrained Phase')
xlabel('Time (s)')
ylabel('Pore pressure (kpa)')
legend('sensor1','sensor2','sensor3','sensor4','sensor5','sensor6','sensor7
',...
```

```
    'sensor8','sensor9','sensor10','base sensor south','base sensor
middle','base sensor north',...
    'Location','southeastoutside')

%% Plotting pore pressure (base tank) and acceleration to determine
undrained phase

plotyy(time1,base_sensor_s,time1,fl_sensor1_accx)
hold on
plotyy(time1,base_sensor_m,time1,fl_sensor1_accy)
hold on
plotyy(time1,base_sensor_n,time1,fl_sensor1_accz)

%%
figure
hold on
yyaxis left
% plot(time1,base_sensor_s,'-b')
plot(time,base_sensor_m,'-b')
% plot(time1,base_sensor_n,'-b')
ylabel('Pore Pressure (kpa)')
ylim([10 15])
yyaxis right
plot(time,fl_sensor1_accx,'-r')
plot(time,fl_sensor1_accy,'-r')
plot(time,fl_sensor1_accz,'-r')
ylabel('Acceleration (g)')
ylim([-1 1])
xlim([120 140])
xlabel('Time (s) \Deltat undrained=3.25s')
title('Time vs Pore Pressure and Acceleration')
hold on
line([122.15 122.15],[-1 1],'Color','k')
line([125.40 125.40],[-1 1],'Color','k')
legend('Pore Pressure Base Sensor','Acceleration Sensor 1 xyz-
direction','Location','Southeast')
```

9.2 Matlab code pore pressure interpolation

```
%%
% 1 cm of water = 0.9806 kpa
% The reference level is the bottom of the tank, i.e. 127 below waterlevel
% height of sections
sand_x = 0:478; % in cm, from left to right side of the part of interest of
the sand body
water_y = 126:-1:0; % in cm, from top of fluidization grid to water level
u_w_water = 0.09806; %kpa per cm water
tank_length = 478; % length of the tank, not completely considered in the
interpolation (right slope not included)
WL = 127; % water level from bottom of tank
crest_height = 85; % height of sand body from bottom
slope_height = 65; % vertical length of the slope
% slope_length = 114;  horizontal length of slope (216-344cm)
toe_height = 20; % heigth of toe from bottom


% in cm from E6 to E1
% lenght of sections: geometry of sand body before failure
crest_start = 0;
crest_end = 232;
crest_length = crest_end-crest_start;
slope_start = 233;
slope_end = 366;
```

```
slope_length = slope_end-slope_start;
toe_start = 367;
toe_end = 478;
toe_length = toe_end-toe_start;

slope_gradient = -((crest_height-toe_height)/((slope_length))); % dy/dx
%%% Dimensions of the sand body of interest is from E6 to middle of E3/E2.
%%% This region contains the full crest from E6, the slope, and the toe
between E3/E2.
%%% The other slope between E2 and E1 is not considered in this model.

%% pore pressures known at certain locations in the sand body
PP_WL = zeros(1,length(crest_start:toe_end)) ;
PP_crest = ones(1,crest_length+1)*(WL-crest_height)*u_w_water;
PP_toe = ones(1,toe_length+1)*(WL-toe_height)*u_w_water;
slope_pp_gradient = ((WL-toe_height)-(WL-
crest_height))*u_w_water/slope_length;
% every 1 cm in x-direction means an increase 0f 0.58 kpa in pressure
PP_slope = PP_crest:slope_pp_gradient:PP_toe; % for every dy=1 cm  and
dx=1.68 cm

%% Defining the location of the zero pore pressure level (WL)

PP_WL_x = crest_start:toe_end;
PP_WL_y = ones(1,length(PP_WL_x))*WL;

%% coordinates of the pressure development along the x and y axis of the
sand body.
% Needed for the known points in the interpolation

% crest
PP_crest_x = crest_start:crest_end;
PP_crest_y = ones(1,crest_length+1).*crest_height;

% toe
PP_toe_x = toe_start:toe_end;
PP_toe_y = ones(1,toe_length+1).*toe_height;

% slope
PP_slope_x = slope_start:slope_end;
PP_slope_y = crest_height:slope_gradient:toe_height;



%% Defining the pore pressures at the right side of the slope and above the
toe. At these hydrostatic conditions are followed.
% these pore pressure are the same at the same height on the slope and can
% be extended to the right boundary at the end of the toe (till
% 347cm)

extended_part_x = toe_end-(slope_start):-1:toe_end-toe_start+2; % give x-
coordinates to the area next to the slope and above the toe


%% Defining the water pressure is the right part in the water (not in the
sand body), hydraustatic conditions are applied
PP_extended = [];
for i = 1:length(PP_slope)-1
    n1 = extended_part_x(i);
    pressure_xy = repelem(PP_slope(i),n1);
```

```
    PP_extended = [PP_extended,pressure_xy];
end

%% The locations of the water pressures above has to be defined. The water
pressures are stored in one row vector,
% beacuse this is necessary for the interpolation function. We use the same
% coordinates for the extented part as for the slope. The range of x-axis
% is extended to the right of the slope.

extended_x = slope_start+1:1:toe_end; % x axis from right side of slope to
end of tank (217cm to 347cm)

PP_extended_x = [];
for j = 1:length(PP_slope)-1
    coordinates_x = extended_x(j:end);
    PP_extended_x = [PP_extended_x,coordinates_x];
end

%% More for y coordinates

extended_x = slope_start+1:1:toe_end; % x axis from right side of slope to
end of tank (217cm to 347cm)

PP_extended_y = [];
for k = 1:length(PP_slope)-1
    n2 = extended_part_x(k);
    coordinates_y = repelem(PP_slope_y(k),n2);
    PP_extended_y = [PP_extended_y,coordinates_y];
end

%% Base injection, so over the whole base one pressure

PP_base_x = 0:1:length(sand_x)-1; %along bottom length of the tank
PP_base_y = zeros(1,length(sand_x)); %bottom is at 0 cm 'height'
PP_base = ones(1,length(sand_x)).*base_sensor_m(1);


%% Defining the locations of the sensors in the tank. These includes the
floating sensors, base sensors and wall sensors.
% TSensor 1,2,3,4,5,6,7,8,9,10.
PP_fl_sensors_x = [275,275,254,254,254,190,190,190,125,125];
PP_fl_sensors_y =
[16.58,48.81,45.95,38.71,9.14,71.04,50.23,35.04,70.42,31.77];
extra_z = [20,20,20,20,20,20,20,20,20,20];

%% Defining the values and the locations of the sensors, these are also
known values at certain point,
% so we can add them to the vector with all the known values.
% To use the interpolation function, we have to create two vectors
% Vector 1 contains the known values (they are all put in de PP_....
% vectors.
% Vector 2 contains the locatoins of the known values (the are all put in
% the PP_..._x/y vector

% PP_all_values = [PP_WL,PP_crest,PP_slope,PP_toe,PP_extended,]';
PP_all_coordinates_x =
[PP_WL_x,PP_crest_x,PP_slope_x,PP_toe_x,PP_extended_x,PP_fl_sensors_x,PP_ba
se_x];
PP_all_coordinates_y =
[PP_WL_y,PP_crest_y,PP_slope_y,PP_toe_y,PP_extended_y,PP_fl_sensors_y,PP_ba
se_y];
```

```
% The coordinates have to been stored in a matrix of two column vectors, so
first we have to put them in the right order:
PP_all_coordinates_xy = [PP_all_coordinates_x',PP_all_coordinates_y'];
% PP_all_values =
[PP_WL,PP_crest,PP_slope,PP_toe,PP_extended,fl_sensor1_p(1),fl_sensor2_p(1)
,fl_sensor4_p(1),...
%
fl_sensor5_p(1),fl_sensor6_p(1),fl_sensor7_p(1),fl_sensor8_p(1),fl_sensor9_
p(1),fl_sensor10_p(1),PP_base]';
%% Subtracting the hydraustatic initial conditions from it
% time = 1:length(fl_sensor2_p);
% figure()
% hold on
PP_all_values =
[PP_WL,PP_crest,PP_slope,PP_toe,PP_extended,fl_sensor1_p(1),fl_sensor2_p(1)
,fl_sensor3_p(1),...

fl_sensor4_p(1),fl_sensor5_p(1),fl_sensor6_p(1),fl_sensor7_p(1),fl_sensor8_
p(1),fl_sensor9_p(1),fl_sensor10_p(1),PP_base]';
PP_all_coordinates_xy = [PP_all_coordinates_x',PP_all_coordinates_y'];
PP_interpolation =
scatteredInterpolant(PP_all_coordinates_xy,PP_all_values,'natural');
[X,Y] = meshgrid([0:length(sand_x)-1],[0:length(water_y)-1]);
Interp_PP0 = PP_interpolation(X,Y);
PP_interpolation.ExtrapolationMethod = 'none';
% surf(X,Y,Interp_PP0,'EdgeColor','none','LineStyle','none')
[C,H] = contour(X,Y,Interp_PP0,'b'); % creating contour lines
clabel(C,H);
hold on
plot3([PP_crest_x,PP_slope_x,PP_toe_x],[PP_crest_y,PP_slope_y,PP_toe_y],[PP
_crest_y,PP_slope_y,PP_toe_y],'k','LineWidth',2)
hold on
scatter3(PP_fl_sensors_x,PP_fl_sensors_y,extra_z,'k','filled')
xlabel('Length of the tank S->N (cm)')
ylabel('Height of the waterlevel (cm)')
title('Pore Pressure Interpolation Through The Sand (Hydrostatic)')
view(0,90)




%% Animated plot of the total pore pressure distribution

for t=1:length(fl_sensor1_p);
fig = figure()
time2 =(t-1)*25
cla
PP_base = ones(1,length(sand_x)).*base_sensor_m(t);
PP_all_values =
[PP_WL,PP_crest,PP_slope,PP_toe,PP_extended,fl_sensor1_p(t),fl_sensor2_p(t)
,fl_sensor3_p(t),fl_sensor4_p(t),...

fl_sensor5_p(t),fl_sensor6_p(t),fl_sensor7_p(t),fl_sensor8_p(t),fl_sensor9_
p(t),fl_sensor10_p(t),PP_base]';
PP_all_coordinates_xy = [PP_all_coordinates_x',PP_all_coordinates_y'];
PP_interpolation =
scatteredInterpolant(PP_all_coordinates_xy,PP_all_values,'natural');
[X,Y] = meshgrid([0:length(sand_x)-1],[0:length(water_y)-1]);
Interp_PP = PP_interpolation(X,Y);
title(sprintf('%1.f ms after base triggering',time2));
surf(X,Y,Interp_PP,'EdgeColor','none','LineStyle','none')
grid on
```

```
[C,H] = contour(X,Y,Interp_PP,'b'); % creating contour lines
clabel(C,H);
hold on
plot3([PP_crest_x,PP_slope_x,PP_toe_x],[PP_crest_y,PP_slope_y,PP_toe_y],[PP
_crest_y,PP_slope_y,PP_toe_y],'k','LineWidth',2)
hold on
scatter3(PP_fl_sensors_x,PP_fl_sensors_y,extra_z,'k','filled')
title(sprintf('%1.f ms after base triggering',time2));
xlabel('Length of the tank S->N (cm)')
ylabel('Height of the waterlevel (cm)')
view(0,90)
drawnow
grid off
saveas(fig,'FIG','png')
end
%% Excess pore pressure interpolation
for t=1:length(fl_sensor1_p);
fig = figure()
time2 =(t-1)*250
cla
PP_base = ones(1,length(sand_x)).*base_sensor_m(t);
PP_all_values =
[PP_WL,PP_crest,PP_slope,PP_toe,PP_extended,fl_sensor1_p(t),fl_sensor2_p(t)
,fl_sensor3_p(t),fl_sensor4_p(t),...

fl_sensor5_p(t),fl_sensor6_p(t),fl_sensor7_p(t),fl_sensor8_p(t),fl_sensor9_
p(t),fl_sensor10_p(t),PP_base]';
PP_all_coordinates_xy = [PP_all_coordinates_x',PP_all_coordinates_y'];
PP_interpolation =
scatteredInterpolant(PP_all_coordinates_xy,PP_all_values,'natural');
[X,Y] = meshgrid([0:length(sand_x)-1],[0:length(water_y)-1]);
Interp_PP1 = PP_interpolation(X,Y);
Interp_exPP = Interp_PP1-Interp_PP0;
surf(X,Y,Interp_exPP,'EdgeColor','none','LineStyle','none')
hold on
plot3([PP_crest_x,PP_slope_x,PP_toe_x],[PP_crest_y,PP_slope_y,PP_toe_y],[PP
_crest_y,PP_slope_y,PP_toe_y],'k','LineWidth',2)
hold on
scatter3(PP_fl_sensors_x,PP_fl_sensors_y,extra_z,'k','filled')
title(sprintf('Excess pore pressure %1.f ms after base triggering',time2));
xlabel('Length of the tank S->N (cm)')
ylabel('Height of the waterlevel (cm)')
col = colorbar
set(col,'ylim',[0 2])
colorbar
view(0,90)
drawnow
end

%% Setting up profile for the total stress 'TS' of the sand body in the
tank
% UW_sand =  unit weight sand
G = 2.67; Se = 1; e = 0.874;
sat_u_w_sand = ((G + e)*u_w_water)/(1+e); % in kpa for every cm of soil in
depth
TS_WL = zeros(1,length(crest_start:toe_end));
TS_crest = ones(1,crest_length+1)*(WL-crest_height)*u_w_water;
TS_toe = ones(1,toe_length+1)*(WL-toe_height)*u_w_water;
TS_slope = PP_crest:slope_pp_gradient:PP_toe;
TS_boundary = [TS_crest,TS_slope,TS_toe];
%% Total stresses in the soil, by using saturated unit weight and the
height of a 1cm column
```

```
TS_crest_bot =
ones(1,length(crest_length))*(TS_crest+(sat_u_w_sand*(crest_height)));
TS_toe_bot =
ones(1,length(toe_length))*(TS_toe+(sat_u_w_sand*(toe_height)));

TS_slope_bot = zeros(1,length(TS_slope));
for h = 1:length(TS_slope)
    TS_slope_bot(h) = TS_slope(h) + (sat_u_w_sand*(PP_slope_y(h)));
end

%% coordinates of the total stress 'TS' development along the x and y axis
of the sand body.
% water level
TS_WL_x = crest_start:toe_end;
TS_WL_y = ones(1,length(PP_WL_x))*WL;
% crest
TS_crest_x = crest_start:crest_end;
TS_crest_y = ones(1,crest_length+1).*crest_height;
% crest bottom
TS_crest_bot_x = crest_start:crest_end;
TS_crest_bot_y = zeros(1,crest_length+1);
% toe
TS_toe_x = toe_start:toe_end;
TS_toe_y = ones(1,toe_length+1).*toe_height;
% toe bottom
TS_toe_bot_x = toe_start:toe_end;
TS_toe_bot_y = zeros(1,toe_length+1);
% slope
TS_slope_x = slope_start:slope_end;
TS_slope_y = crest_height:slope_gradient:toe_height;
% slope bottom
TS_slope_bot_x = slope_start:slope_end;
TS_slope_bot_y = zeros(1,length(crest_height:slope_gradient:toe_height));
TS_bottom = [TS_crest_bot,TS_slope_bot,TS_toe_bot];

TS_bottom_x = [TS_crest_bot_x,TS_slope_bot_x,TS_toe_bot_x];
TS_bottom_y = [TS_crest_bot_y,TS_slope_bot_y,TS_toe_bot_y];
TS_boundary_x = [TS_WL_x,TS_crest_x,TS_slope_x,TS_toe_x];
TS_boundary_y = [TS_WL_y,TS_crest_y,TS_slope_y,TS_toe_y];
%% Putting all the total pressure in one array
TS_all_values = [TS_WL,TS_crest,TS_slope,TS_toe,TS_bottom]';
TS_all_coordinates_x = [TS_boundary_x,TS_bottom_x];
TS_all_coordinates_y = [TS_boundary_y,TS_bottom_y];
TS_all_coordinates_xy = [TS_all_coordinates_x',TS_all_coordinates_y'];
%%
TS_interpolation =
scatteredInterpolant(TS_all_coordinates_xy,TS_all_values,'natural');
[X,Y] = meshgrid([0:length(sand_x)-1],[0:length(water_y)-1]);
TS_Interp = TS_interpolation(X,Y);
% surf(X,Y,TS_Interp,'EdgeColor','k','LineStyle','none')
[C,H] = contour(X,Y,TS_Interp,'b')
clabel(C,H)
hold on
plot3([TS_crest_x,TS_slope_x,TS_toe_x],[TS_crest_y,TS_slope_y,TS_toe_y],[TS
_crest_y,TS_slope_y,TS_toe_y],'k','LineWidth',2)
title('Vertical total stress')
xlabel('Length of the tank (cm)')
ylabel('Height of the waterlevel')
view(0,90)

%%
%% Animated plot of the total pore pressure distribution
```

```
for t=1:length(fl_sensor1_p);
fig = figure()
time2 =(t-1)*25
cla
PP_base = ones(1,length(sand_x)).*base_sensor_m(t);
PP_all_values =
[PP_WL,PP_crest,PP_slope,PP_toe,PP_extended,fl_sensor1_p(t),fl_sensor2_p(t)
,fl_sensor3_p(t),fl_sensor4_p(t),...

fl_sensor5_p(t),fl_sensor6_p(t),fl_sensor7_p(t),fl_sensor8_p(t),fl_sensor9_
p(t),fl_sensor10_p(t),PP_base]';
PP_all_coordinates_xy = [PP_all_coordinates_x',PP_all_coordinates_y'];
PP_interpolation =
scatteredInterpolant(PP_all_coordinates_xy,PP_all_values,'natural');
[X,Y] = meshgrid([0:length(sand_x)-1],[0:length(water_y)-1]);
Interp_PP = PP_interpolation(X,Y);
Interp_ES = TS_Interp - Interp_PP;
surf(X,Y,Interp_ES,'EdgeColor','none','LineStyle','none')
% [C,H] = contour(X,Y,Interp_ES,8,'b'); % creating contour lines
% clabel(C,H);
hold on
plot3([PP_crest_x,PP_slope_x,PP_toe_x],[PP_crest_y,PP_slope_y,PP_toe_y],[PP
_crest_y,PP_slope_y,PP_toe_y],'k','LineWidth',2)
hold on
scatter3(PP_fl_sensors_x,PP_fl_sensors_y,extra_z,'k','filled')
title(sprintf('Vertical effective stress %1.f ms after base
triggering',time2));
xlabel('Length of the tank S->N (cm)')
ylabel('Height of the waterlevel (cm)')
view(0,90)
drawnow
end
```

9.3 Excel for localizing sensors

WL (W5)	126		kpa	1
Air_pressure	101,83		cm	10,1972
Sensors	**Total P (inc atm.)**	Water P (ex. Atm.)	cm of water column	**cm from bot (Y)**
fl_1	112,62	10,73	109,415956	16,584044
fl_2	115	7,57	77,192804	48,807196
fl_3	109,73	7,85	80,04802	45,95198
fl_4	110,4	8,56	87,288032	38,711968
fl_5	113,325	11,46	116,859912	9,140088
fl_6	107,22	5,39	54,962908	71,037092
fl_7	110,75	7,43	75,765196	50,234804
fl_8	109,28	8,92	90,959024	35,040976
fl_9	107,3	5,45	55,57474	70,42526
fl_10	111,07	9,24	94,222128	31,777872
Sensors	**X_dir (S->N)**	**Z_dir (E->W)**		
fl_1	275	110		
fl_2	275	110		
fl_3	254	100		
fl_4	254	100		
fl_5	254	100		
fl_6	190	100		
fl_7	190	100		
fl_8	190	100		
fl_9	125	100		
fl_10	125	100		